BNL-67610

Update
E923 - Search for T Violating Muon Polarization in $K^+ \to \mu^+\pi^o\nu_\mu$ Decay.

October 1, 1998

A. Carroll, M. V. Diwan, J. Frank, A. Gordeev, S. Kettell, L. Leipuner, L. Littenberg, Hong Ma, K. Olchanski, V. Polychronakos
Brookhaven National Laboratory, Long Island, NY

G. Atoyan, Y. Andreev, V. Issakov, O. Karavichev, T. Karavicheva, A. Poblaguev, A. Proskuryakov
Institute for Nuclear Research, Moscow, Russia

V. Semenov
Institute for High Energy Physics, Protvino, Russia

M. Elaasar, D. Greenwood, K. Johnston
Louisiana Tech University, Ruston, LA

R. Adair, R. Larsen
Yale University, New Haven, CT

Experimental Equipment:

Beamline:	D6 2.0 GeV/c Separated K^+ Beam 2.0×10^7 per AGS Pulse
Detector:	Plastic Scintillator, Lead-Scintllator Calorimeter Array,
	Fe shield, Graphite Polarimeter, Tracking chambers
Flux Requested:	2×10^6 AGS pulses at 30×10^{12} Protons/pulse.
	Approximately 2000 hrs of running.

Contact Persons:
Robert Adair, Yale University, adair@yalph2.physics.yale.edu 203-432-3370
Milind V. Diwan, Brookhaven National Laboratory, diwan@bnl.gov 516-344-3327
Hong Ma, Brookhaven National Laboratory, hma@bnl.gov 516-344-2919

BLANK PAGE

Contents

List of Figures

List of Tables

ABSTRACT

This is an update to the E923 proposal for a new search for the time reversal violating polarization of the muon normal to the decay plane of the $K^+ \to \mu^+ \pi^0 \nu$ decay. The value of such polarization in the Standard Model is zero. However, it is now accepted that the baryon asymmetry of the universe requires a source of CP violation stronger than that embodied in the quark mixing matrix. Models of non-standard CP violation that produce the baryon asymmetry could also produce effects observable in the transverse polarization. The very high sensitivity of the experiment makes this search interesting and timely.

In this update we discuss the possibility of additional kaon decay measurements with the same apparatus as well as the detector development over the last year. In particular, we show that we will be able to measure the T-violating muon polarization in $K^+ \to \mu^+ \nu \gamma$ decays. Such a measurement is complimentary to the main goal of this experiment. We also show that we will obtain a large sample of $K^+ \to \pi^+ \pi^0 \gamma$ events that can be used to understand kaon structure and test the detailed predictions from Chiral Perturbation Theory.
"This research supported in part by the U.S. Department of Energy under Contract DE-AC02-98CH10886".

1 Introduction

This is an update to the proposal for a new search for the time reversal violating polarization of the muon normal to the decay plane of the $K^+ \to \mu^+\pi^0\nu$ decay. The value of such polarization in the Standard Model is zero. However, it is now accepted that the baryon asymmetry of the universe requires a source of CP violation stronger than that embodied in the quark mixing matrix. Models of non-standard CP violation that produce the baryon asymmetry could also produce effects observable in the transverse polarization. The very high sensitivity of the experiment makes this search interesting.

We summarize the sensitivity to the $K^+ \to \pi^0\mu^+\nu$ transverse polarization below: The experiment will be performed with in-flight decays in an intense ($2 \times 10^7 K^+$ per pulse) 2 GeV/c separated kaon beam in an existing beam-line at the AGS. The center piece of the detector will be a new polarimeter which will consist of 96 carbon wedges, with active detector elements (either scintillator or wire chambers) between the wedges, arranged in a cylindrical manner around the kaon beam. We expect to analyze more than 10^9 events to obtain sensitivity to the T-violating polarization of ± 0.00013 at 1 sigma, corresponding to the sensitivity of ± 0.0007 to $Im\xi$, an improvement by approximately 40 over the previous best limit. To achieve this level of sensitivity careful attention must be paid to the systematic effects in the experiment. Most of the development since the proposal has gone towards this end.

The proposal for E923 was submitted to the BNL-HENP PAC in October 1996. It was given scientific approval by the laboratory. The experiment was further reviewed by a technical review panel of experts from inside and outside the laboratory; they were charged to examine the technical feasibility of the experiment. The review was chaired by Sam Aronson. This review occurred in January 1997; the technical review panel declared that the technical design of the experiment was sound and did not find any major faults. Nevertheless, they identified a number of items that needed further work. We have tried to address all of these issues.

While the main conclusions regarding the sensitivity of the experiment remain unchanged, in this update we would like to describe some of the development we have performed over the last year to bring the project to the construction stage. We will describe the development regarding the polarimeter alignment, active detector technology, and magnetic field issues. We will also discuss the calorimeter development and the trigger and data acquisition systems.

In addition to the detector development we have also worked on other physics channels

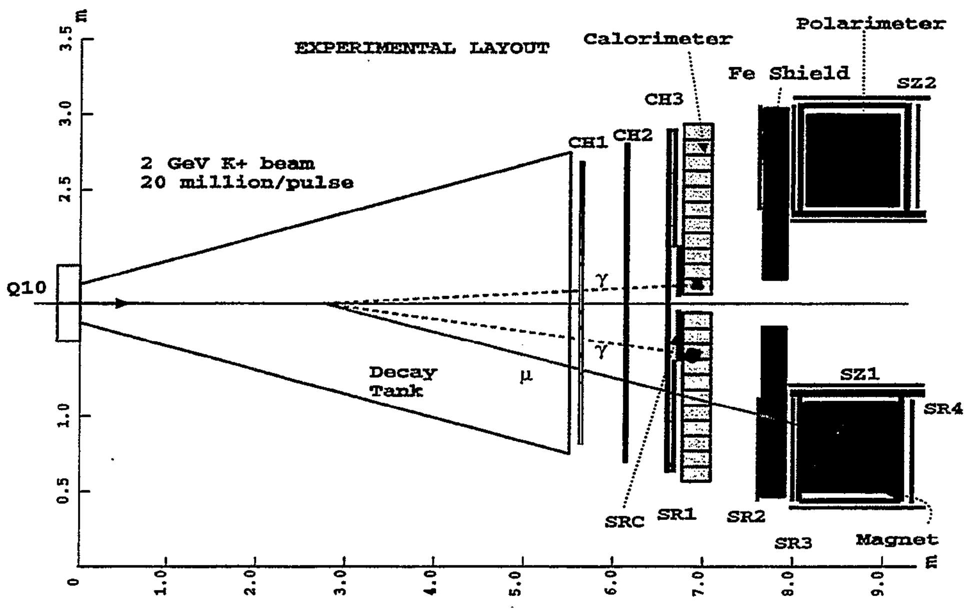

Figure 1: *Schematic of the detector. A typical* $K^+ \to \mu^+\pi^0\nu$ *events is superimposed.*

that can be addressed in the same apparatus. There was some preliminary investigation of the T-violating muon polarization in $K^+ \to \mu^+\nu\gamma$ decays in the E923 proposal. We have extended this study and found ways to improve the sensitivity to this mode.

We have also studied the decay $K^+ \to \pi^+\pi^0\gamma$ to understand the sensitivity in our apparatus. This decay is interesting in the context of modern theoretical methods (Chiral Perturbation Theory or CHPT) that allow detailed predictions of the Dalitz distribution and the photon spectrum including the structure dependent radiation. We would like to obtain a large sample of these events with low background in kinematic regions not explored in previous experiments. With this data better knowledge of the parameters of CHPT can be obtained.

E923 simulation studies are well documented in a series of internal notes [2].

2 $K^+ \to \mu^+\pi^0\nu$ Decay

In this section we would like to summarize our approach to the main goal of this experiment and the subsequent work that has taken place. The E923 experiment will be performed with 2 GeV/c electro-statically separated charged kaons decaying in flight (Fig. 1). The beam intensity will be $2 \times 10^7 K^+$'s/spill with 3×10^{13} protons on target every 3.6 sec. Figure 1 shows the plan view of the experiment. The basic workings of the experiment are the same as the experiment in Ref. [1]. The detailed design is, however, optimized for a high intensity 2 GeV beam. The cylindrically symmetric detector is centered on the kaon beam. The $K^+_{\mu 3}$ decays of interest occur in the decay tank; the photons from the π^0 decay are detected in the calorimeter; the muon stops in the polarimeter. The decay of the stopped muon is detected in the polarimeter by wire chambers or scintillation counters, which are arranged radially between graphite wedges that serve as absorber medium. The hit pattern in the polarimeter identifies the muon stop as well as positron direction relative to the muon stop. By selecting events with π^0 moving along the beam direction and muon moving perpendicular to the beam direction in the K^+ center of mass frame, the decay plane coincides with the radial wedges. A non-zero transverse muon polarization causes an asymmetry between the number of muons that decay clockwise versus the number counter-clockwise. To reduce systematic errors, a weak solenoidal magnetic field along the beam direction (70 gauss or a precession period of $\sim 1\mu s$) with polarity reversal every spill is applied to the polarimeter. If there is an initial muon transverse polarization, there will be a shift in the phase of the sinusoidal oscillation in the measured asymmetry. The difference in the asymmetry for the two polarities is proportional to the T-conserving muon polarization in the decay plane, while the sum is proportional to the T-violating muon polarization normal to the decay plane. Both components will have the same frequency but will be 90 degrees apart in phase. Thus the signal will appear as a $\cos \omega t$ oscillation with the amplitude proportional to the T-violating polarization. The allowed polarization will also be observed as a $\sin \omega t$ oscillation. Therefore the experiment will have an internal check for the analyzing power and background level.

Compared to the previous in-flight experiment, this experiment has higher acceptance, much better background rejection and event reconstruction. The separated K^+ beam should greatly reduce the accidental rate. The polarimeter is finely segmented and the analyzing power is higher. The positron signature is defined by the coincidence of signals in a pair of neighboring wedges. The larger calorimeter makes it possible to measure both photons and to reconstruct the π^0 momentum for a large fraction of the events. Together with the muon trajectory, the events can be fully reconstructed. The detector acceptance and background rejection is optimized using full GEANT simulations.

The experiment will collect approximately 550 events per AGS pulse per 3.6 seconds. Thus the statistical accuracy of the polarization measurement in a 2000 hr (2×10^6 pulses) run will be:

$$\delta P_T \approx \frac{1.20^{\frac{1}{2}}2^{\frac{1}{2}}}{0.35(2\times 10^6 \cdot 550)^{\frac{1}{2}}} \approx 1.3\times 10^{-4}$$

where $\sqrt{1.2}$, $\sqrt{2}$, 0.35, are dilution factors in the analyzing power due to backgrounds, the precession magnetic field, and the muon decay, respectively. The sensitivity to $Im\xi$ is given by

$$\delta Im\xi \approx \delta P_T/0.2 \approx 7\times 10^{-4}$$

where 0.2 is a kinematic factor that includes the acceptance in the Dalitz plot and the orientation of the decay in the center of mass.

We have performed further simulation and optimization work for $K^+ \to \mu^+\pi^0\nu$. In particular, we have studied the effect of polarimeter granularity, the beam momentum, additional photon veto detectors, and the muon range measurement on the sensitivity of the experiment. All of these effects were studied with full GEANT simulation of the detector.

- Reduction of polarimeter granularity from 120 wedges (used for the numbers quoted above above) to 96 wedges decreases the acceptance for muon decay positrons which must go through thicker wedges. Since the detected positrons are of higher energy, the analyzing power is greater, therefore the overall loss in sensitivity is limited to 15%.

- The D6 separated kaon beam can be operated at lower momentum with higher reliability. We find that lowering the momentum from 2 GeV/c to 1.8 GeV/c will cause loss of acceptance by about 35%, however the accepted events have greater sensitivity to $Im\xi$. Thus the overall loss to the underlying physics sensitivity is only about 5%. Also some of the acceptance can be recovered by changing the thickness of the Fe shield.

- As explained in the proposal the final set of events have about 15% background from $K^+ \to \pi^+\pi^0$ and $K^+ \to \pi^+\pi^0\pi^0$ events for the two photon sample. With additional photon veto and muon range measurement (explained in section 3.2) these backgrounds can be eliminated with little loss in acceptance. This will gain approximately 10% in sensitivity for the two photon sample.

The technical review identified a number of issues; these are dealt with in varying detail below. We would like to list these items with some comments here.

- AGS intensity: E923 would like to have 3×10^{13} protons on target per pulse. At the time of the proposal this was not yet achieved. AGS now delivers this intensity regularly to the C2 line target for experiment E787. Additional shielding requirements for the D6 line have been identified and included in the AGS part of the cost estimate for the experiment.

- Magnetic and thermal effects on the active detectors in the polarimeter: We are making prototypes of these detectors. We have measured the magnetic fields in the vicinity of the experiment to be quite small with small or no time dependent components. This is addressed in more detail below.

- Calorimeter performance: We have prototyped the calorimeter. The results of beam tests are described below.

- Electronics and data acquisition: At the time of the technical review we did not have a design for this system. We now have a detailed design and have prototyped several components.

- Asymmetry from polarized Λ production and subsequent parity violating decays: The technical review panel considered this effect to be quite small. We have calculated that most pions that go through the calorimeter and the Fe shield are below threshold for producing Λ. Moreover the chain of parity violating decays that must occur is quite unlikely.

3 Radiative decay $K^+ \to \mu^+\nu\gamma$

The branching ratio for $K_{\mu 2\gamma}$ decay is $(5.5 \pm 0.28) \times 10^{-3}$ in the particle data book. The decay is mostly dominated by inner bremsstrahlung. Recently, the structure dependent part of the branching ratio (for positive helicity photons) has been measured to be $(1.33 \pm 0.12 \pm 0.18) \times 10^{-5}$ [3].

In the $K_{\mu 2\gamma}$ decay the transverse muon polarization, which is T-violating, can come from interference between the inner bremsstrahlung and the structure dependent part of the decay. It is not only sensitive to new pseudo-scalar interactions, in contrast to $K_{\mu 3}$ decay's sensitivity to new scalar interactions, but also new vector and axial vector interactions. Recent studies [4, 5] have shown that in certain extensions of the Standard Model, there could be large T-violating muon polarization in $K_{\mu 2\gamma}$ decays. And finally, the final state interaction can result in a non-zero transverse polarization, which is yet to be calculated, but could be within the sensitivity of the experiment.

3.1 Physics of $K_{\mu 2\gamma}$ decay

Following the calculations by [5], the $K_{\mu 2\gamma}$ decay is described by "inner bremsstrahlung" (IB) and "structure-dependent" (SD) contributions. The parameters are the kaon decay constant f_K, axial vector form factor F_A and vector form factor F_V. The new physics beyond the SM is introduced as additional terms in Lagrangian

$$\begin{aligned}\mathcal{L} &= -\frac{G_F}{\sqrt{2}} sin\theta_c \bar{s}\gamma^\alpha(1-\gamma_5)u\bar{\nu}\gamma_\alpha(1-\gamma_5)\mu + G_S\bar{s}u\bar{\nu}(1+\gamma_5)\mu + G_P\bar{s}\gamma_5 u\bar{\nu}(1+\gamma_5)\mu \\ &+ G_V\bar{s}\gamma^\alpha u\bar{\nu}\gamma_\alpha(1-\gamma_5)\mu + G_A\bar{s}\gamma^\alpha\gamma_5 u\bar{\nu}\gamma_\alpha(1-\gamma_5)\mu + h.c., \end{aligned} \quad (1)$$

where G_F is the Fermi constant, θ_c is the Cabibbo mixing angle, and G_S, G_P, G_V, and G_A are parameters of the nonstandard model interactions due to scalar, pseudo-scalar, vector, and axial vector boson exchange, respectively.

The new interactions will modify the decay constants and form factors in the following way,

$$\begin{aligned} f_K &= f_K^0\,(1+\Delta_P+\Delta_A)\,, \\ F_A &= F_A^0(1+\Delta_A), \\ F_V &= F_V^0(1-\Delta_V), \end{aligned} \quad (2)$$

and

$$\Delta_{(P,A,V)} = \frac{\sqrt{2}}{G_F sin\theta_c}\left(\frac{G_P m_K^2}{(m_s+m_u)m_\mu}, G_A, G_V\right). \quad (3)$$

The T-violating muon polarization comes from the interference of IB and the imaginary part of the SD, which can only come from pseudo-scalar (G_P) and right-handed current ($G_R = G_V + G_A$).

$$P_T(x,y) = P_T^V(x,y) + P_T^A(x,y) \quad (4)$$

with

$$\begin{aligned} P_T^V(x,y) &= \sigma_V(x,y)[Im(\Delta_A+\Delta_V)]\,, \\ P_T^A(x,y) &= [\sigma_V(x,y)-\sigma_A(x,y)]Im(\Delta_P)\,, \end{aligned} \quad (5)$$

where $\sigma_V(x,y)$ and $\sigma_A(x,y)$ are analytic functions of the Dalitz plot variables ($x = 2E_\gamma/M_K$, $y = 2E_\mu/M_K$).

The T-conserving muon polarization is also given in [5]. In Fig 2, the longitudinal and in-plane normal polarization of the muon are shown on the Dalitz plot, as well as the transverse T-violating muon polarization in terms of σ_V and $\sigma_V - \sigma_A$.

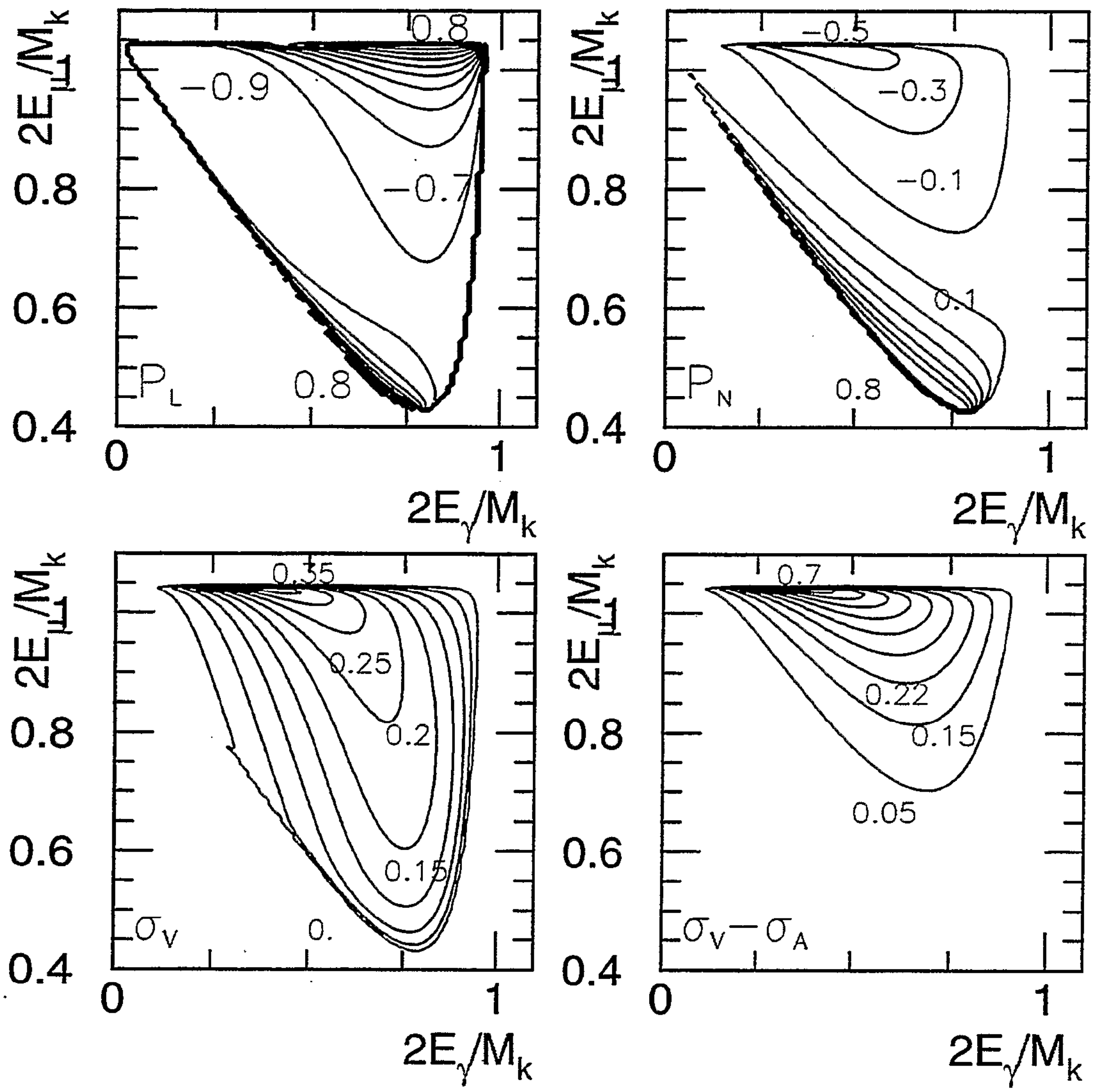

Figure 2: *Muon polarization along the muon momentum (top left), muon polarization normal to muon momentum and in decay plane (top right),* σ_V *(bottom left) and* $\sigma_V = \sigma_A$ *(bottom right) on the Dalitz plot.*

3.2 Detector Enhancement

A set of photon veto counters could be added to detect the second photon from π^0 decays to reject background for $K_{\mu 2\gamma}$ from $K^+ \rightarrow \pi^0\mu^+\nu$ decays. The basic design is a barrel of Pb-scintillator counters surrounding the decay volume, and a ring of counters surrounding the calorimeter perimeter, leaving access to the chambers between the calorimeter and the decay volume. The barrel veto counter extends from z=200 to 550 cm with an inner radius of 94cm. The ring veto counter sits immediately in front of the calorimeter with some overlap, and extends to a radius of 190 cm. The total area of the veto counters is about 28 m^2.

The veto counter consists of sandwiches of 1mm Pb and 2mm plastic scintillator. The total thickness is 16 cm, corresponding to 10 radiation lengths. The sampling fraction is about 15%.

With a threshold of 20 MeV, taking into account only the K^+ decays, the rates in the veto counters will be about 0.078 and 0.04 / K^+ in the barrel and ring veto counters respectively. With $2\times10^7 K^+$'s/sec, the total rate is 2.4 MHz, or 2.4% occupancy with 10 ns time window. The real rate will be higher than this, since this only takes the K^+ decays into account.

The veto counter is not needed for the main goal of the experiment of detecting transverse muon polarization in $K^+ \rightarrow \pi^0\mu^+\nu$ decays. Such a veto counter would be a significant upgrade to the detector. Although, it will add significantly to the sensitivity for $K_{\mu 2\gamma}$ decays, we will also comment on how much of the sensitivity can be obtained without the photon veto.

We have increased the calorimeter depth to 15 radiation lengths (the proposal used 13 radiation lengths) to improve resolution on photons of energy $\sim 1\ GeV$. The shielding behind the calorimeter is reduced to keep the same muon momentum acceptance. We have also used calorimeter resolution of $4\%/\sqrt{E}$. Good calorimeter resolution is important to achieve low background for the radiative decays. However, we have also studied the possibility using calorimeter resolution of $8\%/\sqrt{E}$; there is only moderate loss in the acceptance for these decays. We expect that the real resolution will be between these possibilities. The calorimeter development is described below.

We have assumed that the polarimeter active elements are segmented in 10 divisions (of 10 cm each) along the beam direction. The muon energy acceptance is between 0.5 and 0.8 GeV in the polarimeter. The resolution on the energy from the measurement of range is expected to be about 23 MeV. With a perfect measurement of Z, the resolution would be 17 MeV. Furthermore, for the simulations reported here we have assumed that the polarimeter is made of 96 wedges.

3.3 Event selection

Event selection criteria for $K_{\mu 2\gamma}$ events are:

1. One muon stop signal in the polarimeter;
2. One cluster in the calorimeter with energy over 0.6 GeV, and no other cluster over 50 MeV (excluding cluster associated with the muon);
3. Unambiguous positron signal associated with the stop;
4. $(\text{Missing mass})^2 < 0.01\ (\text{GeV})^2$;
5. Veto counter energy < 20 MeV.

Table 1 summarizes the number of events for different decay modes for 1×10^7 K^+'s before and after the last two cuts. The $K_{\pi 3}$ events are eliminated by the missing mass cut. After the photon veto, the dominant background comes from $K_{\mu 3}$ decays. The signal to background is about 2.2 to 1.

The z-θ cut is not used here because the $K_{\pi 2}$ background is not significant, and the cut would eliminate $K_{\mu 2\gamma}$ events with high muon momentum in the center of mass, which have higher sensitivity to the T-violating polarization.

Figure 3 shows the photon energy and muon energy distributions for the different decay modes. Because of the kinematic limit on the muon momentum for the $K_{\mu 3}$ decay, there exists a region ($E_\mu > 220 MeV$) where the $K_{\mu 3}$ background can be eliminated.

Decay	Cuts(1-3)	Missing mass cut	Photon veto
$\mu^+\nu\gamma$	9.0	7.9	7.8
$\pi^0\mu^+\nu$	48	18	3.2
$\pi^0\pi^+$	2.1	1.2	0.4
$\pi^0\pi^0\pi^+$	3.2	0.02	0

Table 1: *Number of μ-γ events for different decay modes per 1×10^7 K^+ after standard cuts, and additional cuts using muon energy measurement and photon veto ($< 20 MeV$). All cuts are applied successively.*

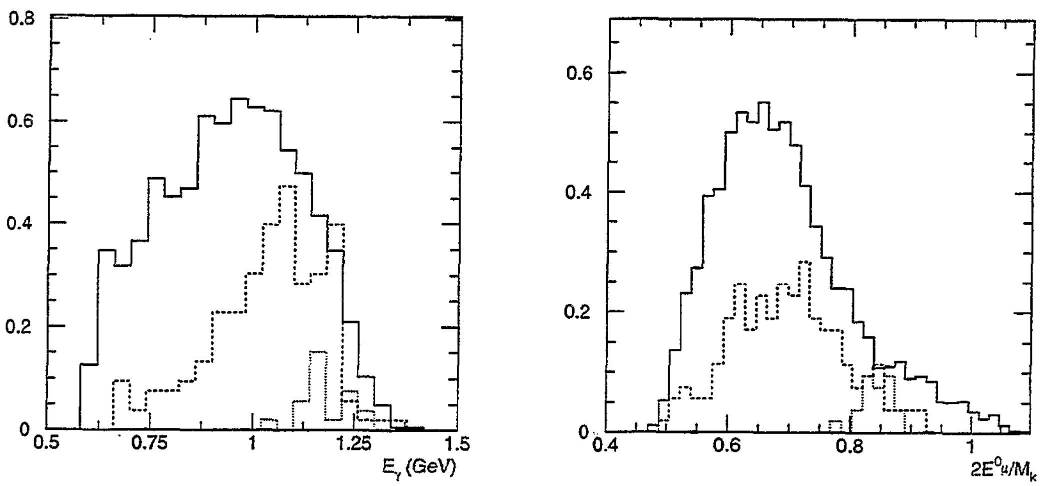

Figure 3: *Left: Photon energy distribution in the lab frame for the accepted events from* $K_{\mu 2\gamma}$ *decays (solid),* $K_{\mu 3}$ *decays (dash) and* $K_{\pi 2}$ *decays (dots). Right: Distribution of the muon energy in the kaon center of mass system with the same notation for different decay modes.*

3.4 Sensitivity

Assuming that there is no T-violation in $K_{\mu 3}$ decay, the background in the $K_{\mu 2\gamma}$ sample only reduces the sensitivity. For 2000 hours of running, we expect to collect 32 million $K_{\mu 2\gamma}$ events. Assuming a background of 50 percent, we can achieve a sensitivity to P_T of

$$\sigma_{P_T} \sim \frac{\sqrt{1.5} \times \sqrt{2}}{0.4\sqrt{32 \times 10^6}} = 7.7 \times 10^{-4}$$

The sensitivity to the new physics depends on the distribution on the Dalitz plot. Figure 4(a) shows the accepted events on $K_{\mu 2\gamma}$ Dalitz plot. Figure 4(b) and (c) show the figure of merit, $P_T \times \sqrt{N}$ on the Dalitz plot for σ_V and $\sigma_V - \sigma_A$. Figure 4(d) shows the distribution of σ_V and $\sigma_V - \sigma_A$ for the accepted events.

The ratios are calculated to be

$$\frac{P_T}{Im(\Delta_R)} = \overline{\sigma_V} = 0.11$$

$$\frac{P_T}{Im(\Delta_P)} = \overline{\sigma_V - \sigma_A} = 0.04$$

Using the error on P_T, the sensitivity to the imaginary part of the form factor can be found:

$$\sigma_{Im(\Delta_R)} = 7 \times 10^{-3}$$

$$\sigma_{Im(\Delta_P)} = 0.02$$

Since the figure of merit varies significantly over the Dalitz plot for $\sigma_V - \sigma_A$, we can eliminate the events with low sensitivity, and improve the overall sensitivity by about a factor of 1.5. For the models considered in [5], our sensitivity is significantly beyond the current bounds on the $P_T(K_{\mu 2\gamma})$ of typically around 10^{-2}.

In principle, even without the photon veto detector, we can select the $K_{\mu 2\gamma}$ events with high muon momentum in the center of mass frame, above the kinematic limit of the $K_{\mu 3}$ decay. This requires good understanding of the kinematic resolutions.

With $2E_\mu/M_K > 0.95$, the estimated number of $K_{\mu 2\gamma}$ events per 10^7 K^+'s is 0.18; the signal to background ratio of 3:1 is expected. The ratios of P_T to the imaginary part of the form factors are calculated to be

$$\frac{P_T}{Im(\Delta_R)} = \overline{\sigma_V} = 0.15$$

$$\frac{P_T}{Im(\Delta_P)} = \overline{\sigma_V - \sigma_A} = 0.25$$

For P interaction, there is little loss of sensitivity because of the increase of $\frac{P_T}{Im(\Delta_P)}$. For right-handed current, this corresponds to a loss of sensitivity by a factor of 4.8.

We have also calculated the sensitivity using $8\%/\sqrt{E}$ for the calorimeter resolution. The resolution of the (missing mass)^2 will be worse by a factor of 1.37. Using the same cuts gives us approximately the same background, but acceptance will be lowered by about 20%, and the the sensitivity will be worse by a factor of 1.15.

It is interesting to note that the T-conserving muon polarization of $K_{\mu 2\gamma}$ decays perpendicular to the precession field is in the opposite direction of that of $K_{\mu 3}$ decays, because the μ^+ is largely left-handed in $K_{\mu 2\gamma}$ decays and right-handed in $K_{\mu 3}$ decays. The magnitude of this polarization depends strongly on the $K_{\mu 3}$ background, and can serve as a check of the purity of the sample.

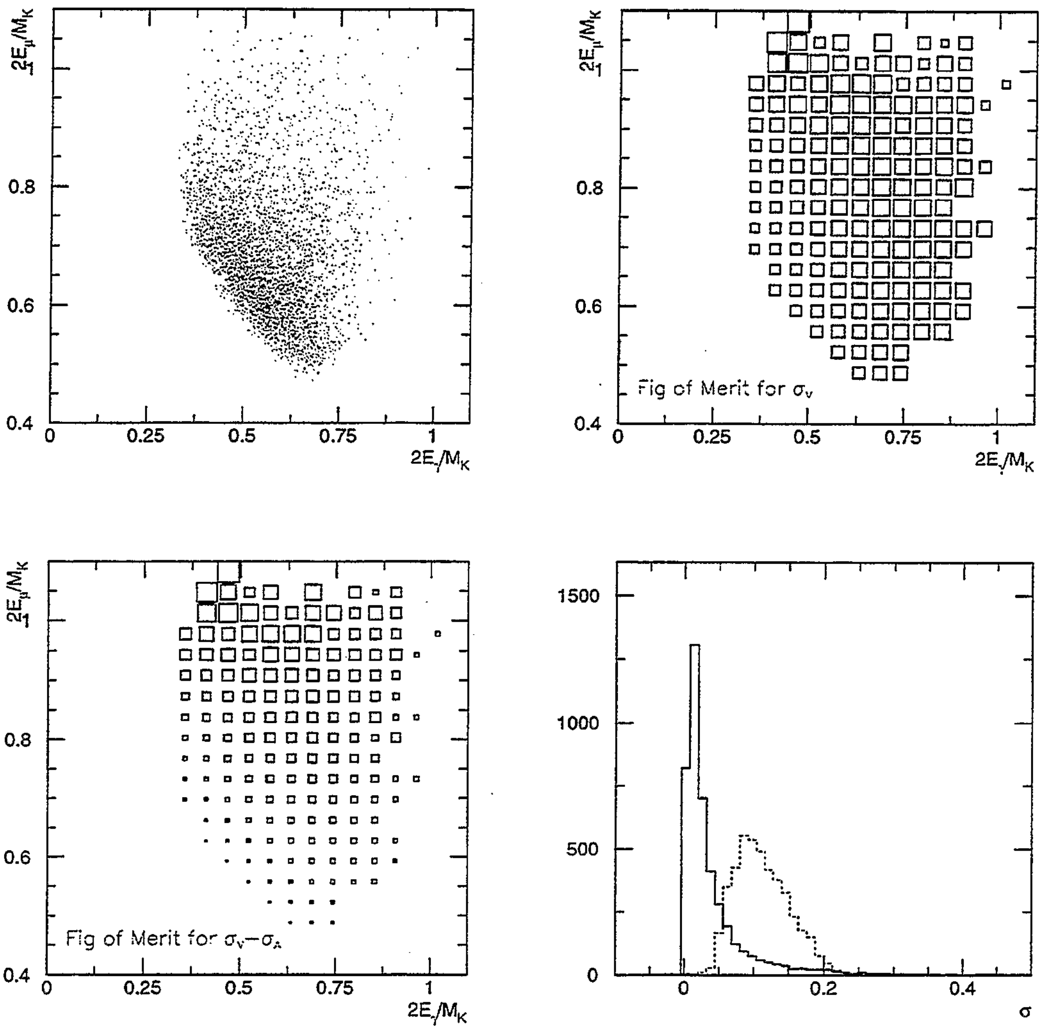

Figure 4: *Top-Left: Dalitz plot of the accepted $K_{\mu 2\gamma}$ events. E_μ and E_γ are measured quantities Lorentz transformed in the kaon center of mass frame; Top-right (bottom-left): figure of merit = $P_T * N^{0.5}$ for σ_V ($\sigma_V - \sigma_A$); Bottom-right: distribution of $\sigma_V - \sigma_A$ (solid) and σ_V(dash) of the accepted events.*

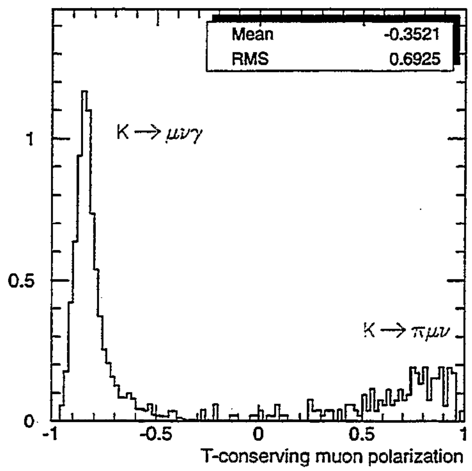

Figure 5: *T-conserving component of muon polarization perpendicular to the precession field for all the accepted events.* $K_{\mu 3}$ *and* $K_{\mu 2\gamma}$ *contributions are indicated on the plot, while the* $K_{\pi 3}$ *background should be flat.*

4 Radiative decay $K^+ \to \pi^+\pi^0\gamma$

Amplitude of $K_{\pi 2\gamma}$ decay can be written in terms of $K_{\pi 2}$ decay in two parts corresponding to the dipole electric (E1) and magnetic (M1) radiation:

$$M_{K\to\pi\pi\gamma} = \frac{ieM_{K\to\pi\pi}}{M_K^4}\varepsilon^\mu \left[iF_E(k^\mu(pq) - p^\mu(kq)) + f_M e^{\mu\nu\alpha\beta}p^\nu k^\alpha q^\beta\right] \tag{6}$$

Here, k, p, and q are 4-momenta of K^+, π^+, and γ, respectively. Form factor F_E includes parts from Inner Bremsstrahlung, unambiguously defined by $K^+ \to \pi^+\pi^0$ amplitude, and structure dependent, f_E, radiation:

$$F_E = \frac{M_K^4}{(pq)(kq)} + f_E \tag{7}$$

In the above we neglect the effects of $\pi\pi$ scattering. Inner Bremsstrahlung does not contribute to the magnetic form factor, which appears due to the chiral anomaly [6]. It is expected that this form factor is dominant in the structure dependent radiation, therefore $K \to \pi\pi\gamma$ decay provides an interesting opportunity to study the chiral anomaly in nonleptonic decays.

The decay probability can be presented as

$$d\Gamma \sim \left[\frac{1}{w^2} + \frac{2f_E}{w} + (f_E^2 + f_M^2)\right] \mathrm{DE}(E_\gamma, \cos\theta_{\pi\gamma}) dE_\gamma d\cos\theta_{\pi\gamma} \quad (8)$$

where $w = M_K^4/(pq)\,(kq)$, E_γ is photon energy in the kaon rest frame, and $\theta_{\pi\gamma}$ is opening angle between photon and charged pion in rest frame of pion pair, and $DE(E_\gamma, \cos\theta_{\pi\gamma})$ is a function of kinematic variables, corresponding to the pure structure dependent radiation. If the form factors are independent of kinematic variables, one can isolate three possible contribution to the decay rate: Inner Bremsstrahlung IB, Interference INT ($\sim f_E$), and Direct Emission DE $\sim (f_E^2 + f_M^2)$.

The Chiral Perturbation Theory relates form factors f_E and f_M to other parameters in the theory; these parameters can be measured in other nonleptonic processes, but are still unknown [6]. One estimate of these parameters gives: $f_E = 13$ and $f_M = 41$ [7]. Measurements of many nonleptonic processes are now needed to understand the detailed predictions of ChPT.

Two previous experimental studies of $K^+ \to \pi^+\pi^0\gamma$ [8] determined the contribution of the structure dependent radiation to be:

$$\mathrm{BR}_{\mathrm{INT+DE}}(55 < T_{\pi^+}(MeV) < 90) = (1.8 \pm 0.4) \times 10^{-5} \quad (9)$$

The first experiment (Abrams et al.) collected ~2100 events with 120 in the direct emission part of the spectrum. The second experiment (Bolotov et al.) collected ~ 140 events with 30 in the direct emission part of the spectrum. Due to low statistics, contributions of INT and DE could not be separated. Supposing that only one form factor contributes to the decay one can estimate

$$f_E = 8.5 \pm 2 \qquad f_M = 0$$

OR

$$f_E = 0 \qquad f_M = 38 \pm 4$$

4.1 Background

The most serious problem in experimental study of $K^+ \to \pi^+\pi^0\gamma$ decay is the background due to the $K^+ \to \pi^+\pi^0\pi^0$ (BR $= 1.7 \times 10^{-2}$) decay with one missed photon. The veto counter described in 3.2 will significantly suppress such background. The remaining background mainly comes from events in which photons are overlapping in the calorimeter. To reduce this background we will apply a cut on the Z-coordinate of the vertex to increase the distance between the decay vertex and the calorimeter.

With perfect kinematic resolutions for $K^+ \to \pi^+\pi^0\pi^0$ decay $M_{\pi\pi\gamma} < 465$ MeV, $M_{\pi\pi} <$ 360 MeV, $p_\pi < 135 MeV$. These kinematic constraints can be used to totally eliminate background if the resolution is good enough. Because we do not measure the π^+ momentum we can actually use only the $\pi\pi\gamma$ constraint. In the following we assume that the calorimeter resolution is $4\%/\sqrt{E}$. A large fraction of the kinematic resolution is the coordinate measurement in the calorimeter, therefore we expect that degradation of the calorimeter resolution will reduce the acceptance by a modest amount.

Because of the high pion momentum for signal events in the kaon rest frame, the pion angle θ_π in the lab frame can also be used to reject background. The measurement of the charged pion opening angle can be performed with high accuracy, and therefore the cut on π^+ opening angle is an important tool for kinematic suppression of $K_{3\pi}$ background.

4.2 Event selection

The event selection criteria for $K_{\pi 2\gamma}$ events are:

1. Three clusters in the calorimeter with total energy over 200 MeV, and no other clusters over 50 MeV (excluding cluster associated with pion)

2. Two photons can be combined with $120 < M_{\gamma\gamma} < 150\ MeV$

3. veto counter energy < 20 MeV

4. π^+ opening angle $\theta_\pi > 270$ mrad

5. z-coordinate of vertex $z_V < 480$ cm

6. Effective mass of decay $490 < M_{\pi\pi\gamma} < 540$ MeV.

The distributions illustrating the effect of the cuts are presented in Fig. 6.

4.3 Expected Results

The distribution of kinematic variables after applying all cuts is presented in Fig. 7. We expect to get 7100 IB events ($E_\gamma > 40\ MeV$), 1100 INT events ($f_E = 8.5$), 1400 DE events ($f_M = 38$), and 150 background events for 2×10^{10} kaons (approximately 1 hour run assuming

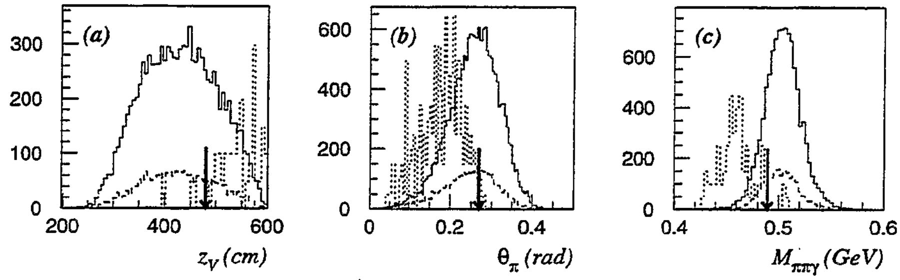

Figure 6: *Normalized distributions for IB (solid), DE (dash), $K_{\pi3}$ (dots). Arrow indicates used cut.*

full detector efficiency). The understanding of the background is currently limited by Monte Carlo statistics; we are in the process of increasing the statistics with better computers. Events with $E_\gamma < 100\ MeV$ and $\cos\theta_{\pi\gamma} > 0$ are dominated by Inner Bremsstrahlung and may be used for absolute normalization, while events with $E_\gamma > 100\ MeV$, $\cos\theta_{\pi\gamma} < 0$ are suitable for detecting contribution of structure dependent radiation (Fig. 8).

We have performed the same calculation for a calorimeter with a resolution of $8\%/\sqrt{E}$. We have retuned the cuts to produce the same level of background; this results in a loss of acceptance for the signal by $\sim 30-40\%$. We will expect to get 4800 IB, 700 INT ($f_E = 8.5$), 900 DE ($f_M = 38$), and 150 background events per hour of running. Because of the huge statistics the physics capability will be approximately the same.

Although the radiative events can clearly be distinguished from background in the experiment, more work needs to be done to understand how to trigger on these events. A trigger that requires 4 clusters in the calorimeter as well as fast online track reconstruction could be sufficient to bring the trigger rate to a manageable level. This is currently being investigated.

The large statistics in E923 experiment will allow us to measure the direct emission branching ratio with $< 5\%$ error. The remaining error will be mostly systematic. Furthermore, we will also be able to distinguish between INT and DE terms. This is demonstrated in Fig. 9 where we have made a fit to the simulated Dalitz plot distribution with $f_E = 13$ and $f_M = 41$. The resolution depends on the value of the form factors; at the assumed values we will obtain a statistical resolution of ± 2 for f_E and ± 3 for f_M based on 1 hour of running. The statistical resolution will improve as $\frac{1}{\sqrt{hours}}$, therefore the final resolution will be dominated by systematics errors. The systematic errors will mainly come from the shape of the background and the variation of the acceptance over the kinematic region. This will

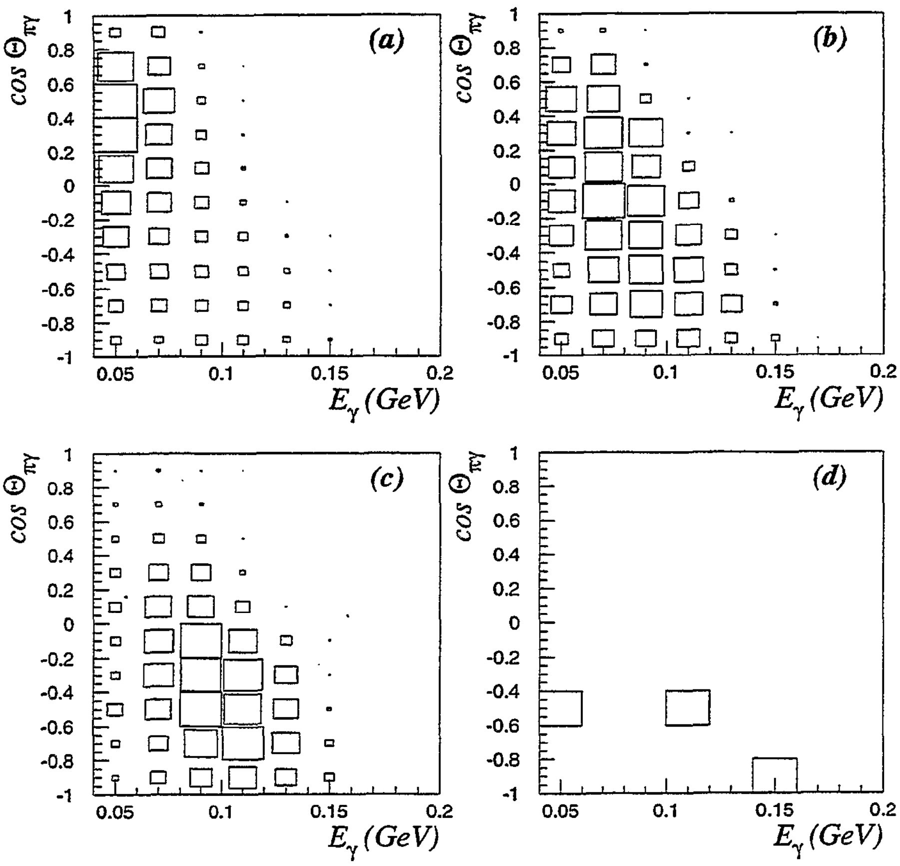

Figure 7: *Photon-pion opening angle* $\cos\theta_{\pi\gamma}$ *versus photon energy* E_γ *in the center of mass. Distributions for (a) Inner Bremstrahlung, (b) Interference, (c) Direct Emission, (d)* $K^+ \to \pi^+\pi^0\pi^0$ *background.*

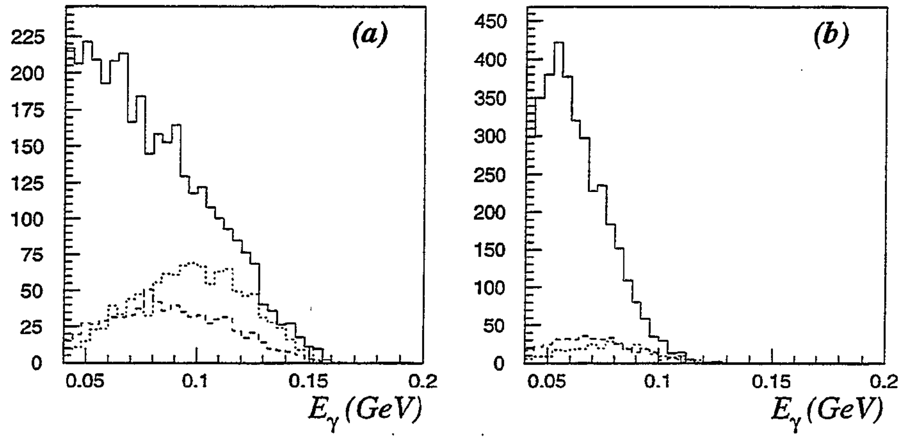

Figure 8: *Expected E_γ distributions, corresponding to* 2×10^{10} K^+ *for IB (solid), INT (dashed), DE (dots) for different cuts: (a)* $\cos\theta_{\pi\gamma} < 0$*; (b)* $\cos\theta_{\pi\gamma} > 0$*;*

be investigated as we proceed with the planning of the experiment.

5 Polarimeter development

The technical review of the experiment on Jan 17, 1997 concluded with a summary of possible systematic errors in the experiment. As explained in the proposal the signal will appear as a $\cos\omega t$ oscillation with the frequency of the muon precession in the magnetic field of the polarimeter. The amplitude of the cosine oscillation will be the T-violating component of the muon polarization. The analysis of the systematic errors is complicated, therefore we will only report the summary of the analysis. The full analysis can found in the internal notes of the E923 collaboration [9] [10]. The systematic errors were divided in several classes:

- A: First order errors that produce a signal as $\cos\omega t$. These are clearly the worst kind of errors that must be reduced below the statistical sensitivity of the experiment. The sources of these errors are:

  (1) Angular misalignment of a wedge with respect to the opposite side wedge. The outside point of a wedge must be aligned with respect to the line through the opposite wedge to within $\pm 0.5mm$ if this error is not correlated over the entire apparatus.

  (2) Clock delay (t_0) of the active detectors in the polarimeter may depend on the direction of the precession field. As described in the proposal the direction of the

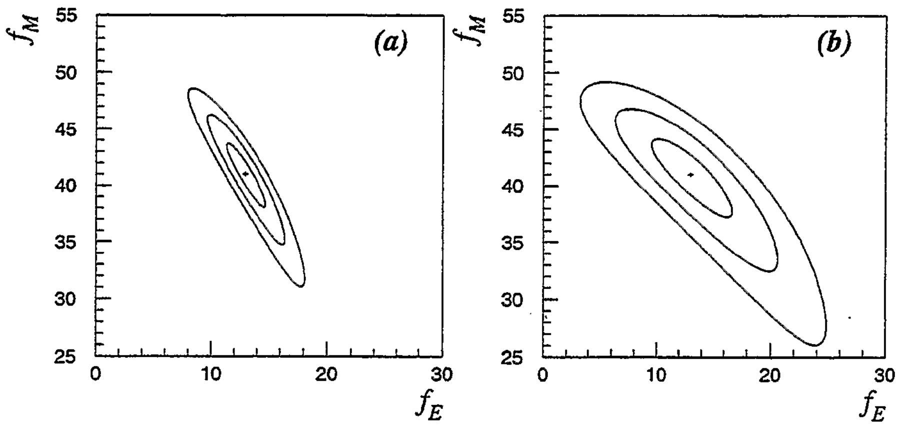

Figure 9: *Expected resolution $f_E = 13$ and $f_M = 41$ from E923 $\sim$ 1 hour statistics. (a) Assumes absolute normalization using the IB part of the Dalitz plot. (b) assumes a fit only to the shape of the Dalitz plot. The contours are 1, 2, 3 sigma.*

precession field is reversed from pulse to pulse to extract the signal. If the effect is random from channel to channel this clock delay needs to be calibrated to within $\pm 300ps$ for each field direction. We believe the PMTs can be shielded very well from the field and the remaining effect can be eliminated by calibration with through-going muons to $\pm 30ps$.

(3) The magnitude of the precession magnetic field changes upon reversal. This causes an asymmetry that grows as $\delta\omega \cdot t/2$ where $\delta\omega$ is the additional precession due to the extra magnetic field in one direction. Although this effect can be distinguished from the real signal through proper analysis, it is best kept small. The asymmetry between the magnitude of the fields must be kept within $6mG$.

(4) Extra longitudinal magnetic fields in the decay region may rotate the muon polarization in flight. The stray longitudinal fields need to be kept below $\sim 1Gauss$.

- B: First order effects that produce a signal as $\sin \omega t$.

Such a situation can arise if the detector efficiency or the polarimeter analyzing power depends on the sign of the precession field. Although the effect is benign, it can be essentially eliminated by proper analysis techniques such as normalizing the numbers of events for each sign of the magnetic field as well as accurately measuring the analyzing

$\frac{\Delta B}{B}\left(\frac{\omega t}{2}\right) \approx 10^{-4}$

$\sim 1 \quad \Rightarrow \Delta B \sim 6\,mG$

power.

- C: Effects that produce a flat asymmetry in time.

  These effects are entirely benign, nevertheless we would like to reduce them to the expected statistical sensitivity. They arise out of

  (1) Unequal clockwise versus counter-clockwise efficiency. This can be eliminated by proper normalization.

  (2) Polarimeter is twisted so that the front and back of the polarimeter are misaligned, and there is a screw like twist. Such a situation causes the longitudinal polarization, not precessing in the field, to project out of the plane. To keep this effect small we will have to align the outer edges of the front and back of the polarimeter to $\sim 150\mu$m.

- D: Second order effects.

  There are a variety of second order effects. Detailed information can be obtained from collaboration internal notes. Most of them do not produce a spurious T-violating effect. Some of them deform the cosine wave. Effects that create a spurious T-violating effect are characterized by two orthogonal misalignments or efficiency gradients. These can be eliminated by performing a more sophisticated analysis of the data than was described in the proposal. For example, if we measure the T violating asymmetries in each opposing pair of wedges and then average over the entire detector most effects will be reduced.

  To keep the second order effects small we must keep the beam, calorimeter, and the polarimeter centered to within 5 mm. The angular alignment of the beam must be controlled within 4 mrad. The detector efficiencies need to kept uniform within 4%. Sophisticated analysis techniques can further relax these conditions.

5.1 Alignment procedure

The polarimeter construction and alignment has be separated into four separate parts. (1) graphite block construction, (2) frame and magnet assembly, (3) graphite block installation and alignment, (4) active detector installation. See Fig. 10.

The most critical part of this process will be the graphite block installation and alignment. To test this process we have constructed a full scale model that can hold 6 graphite blocks (Fig. 11). For the moment, we have tested various concepts for the alignment procedure

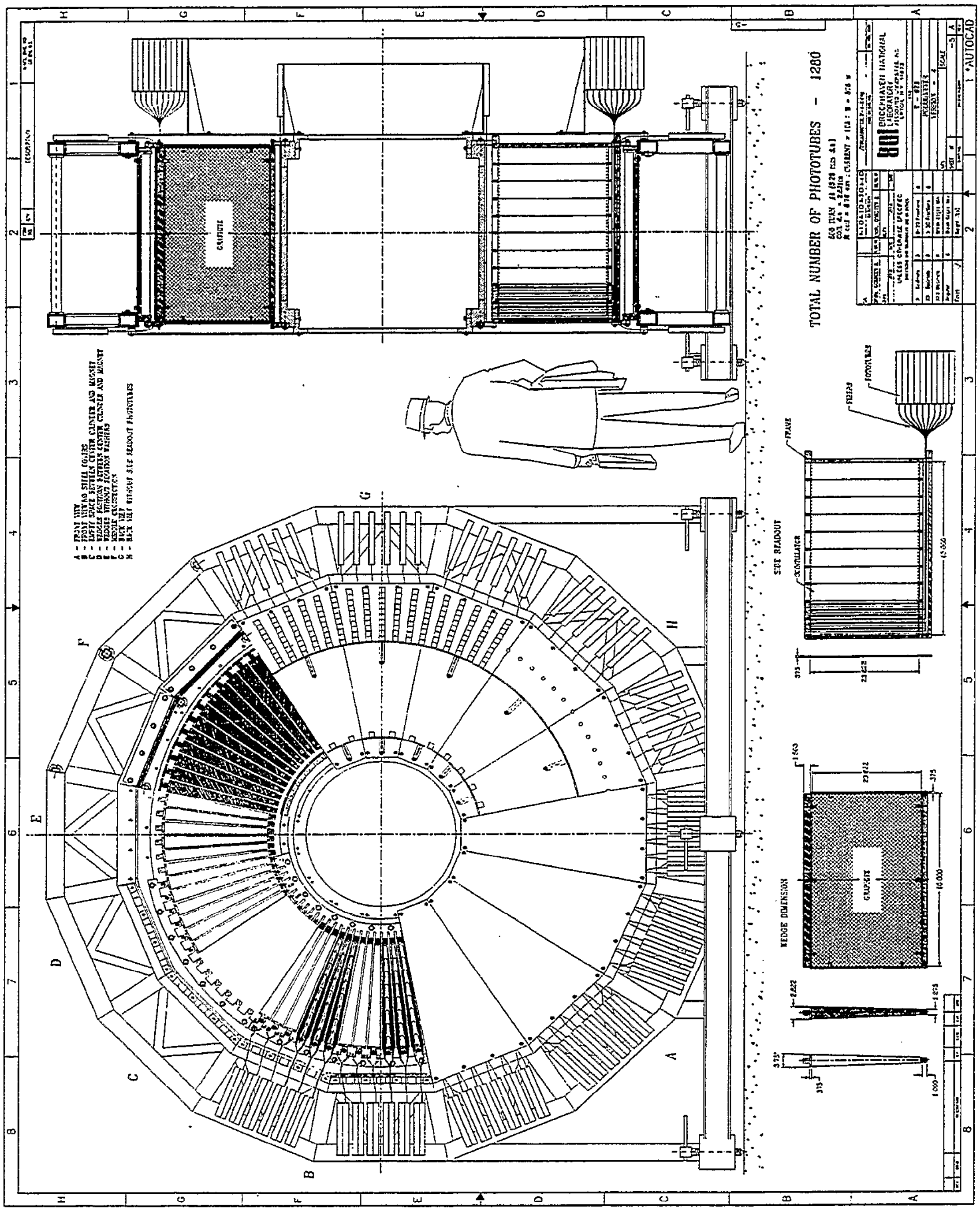

Figure 10: *Preliminary engineering drawing of the polarimeter.*

using precision aluminum plates as substitutes for the graphite blocks. One such procedure is illustrated in Fig. 12. This procedure uses a tensioned steel wire between two precision washers. The polarimeter wedge is rotated until the washer at the pivot point touches the steel wire. This movement of the wedge is performed with a small set-screw and the alignment is observed with a microscope. This procedure is fast and results in alignment accuracy of 0.001 inch. We have so far carried out the procedure with the wire in the horizontal plane, in the future we plan to adapt this procedure to the vertical where gravity will complicate the procedure by making the wire sag slightly.

The polarimeter design shown in Fig. 10 has been influenced by finite element stress model calculations [11]. The graphite wedges are now supported in the polarimeter in such a way that deformities in the supporting structure can be treated separately from the deformities in the graphite wedge. Therefore the structure can be made as strong as needed without affecting the stress on the polarimeter wedges. It is estimated that under their own weight the polarimeter wedges will have insignificant deformation. Furthermore as long as the temperature fluctuations and temperature gradients are kept within ± 2 degree Celsius the joints will not be affected.

5.2 Graphite Wedge manufacturing

The graphite wedges must be manufactured to high precision so that installation and alignment procedure can be carried out with little difficulty. Fig. 13 shows the sketch of a graphite wedge. The critical issue in the graphite manufacturing is the placement of the precision bars. They much be aligned so that the 4 fiducial holes are in the same plane within 0.0005 inch. A manufacturing process has been devised to obtain this precision; the shape of the wedge is machined after the fiducial holes are aligned [12]. We have carried out extensive discussions about the graphite manufacturing with two manufacturers. One of the manufacturers is highly experienced in the production of large blocks of graphite for industrial applications as well as precision machining, and installation of metal hardware in graphite. We expect to work closely with them to assure appropriate quality control.

As part of the polarimeter R&D we tested various industrial graphite materials in a polarized muon test beam and measured the asymmetry. The test was carried out at TRIUMF (Vancouver, Canada) in the M13 surface muon beam by Dr. Syd Kreitzman. We are grateful to Dr. Kreitzman, R. Kiefl, and B. Hitti for the use of their apparatus and expertise. The test was carried out to make sure that the industrial quality graphite has the maximum

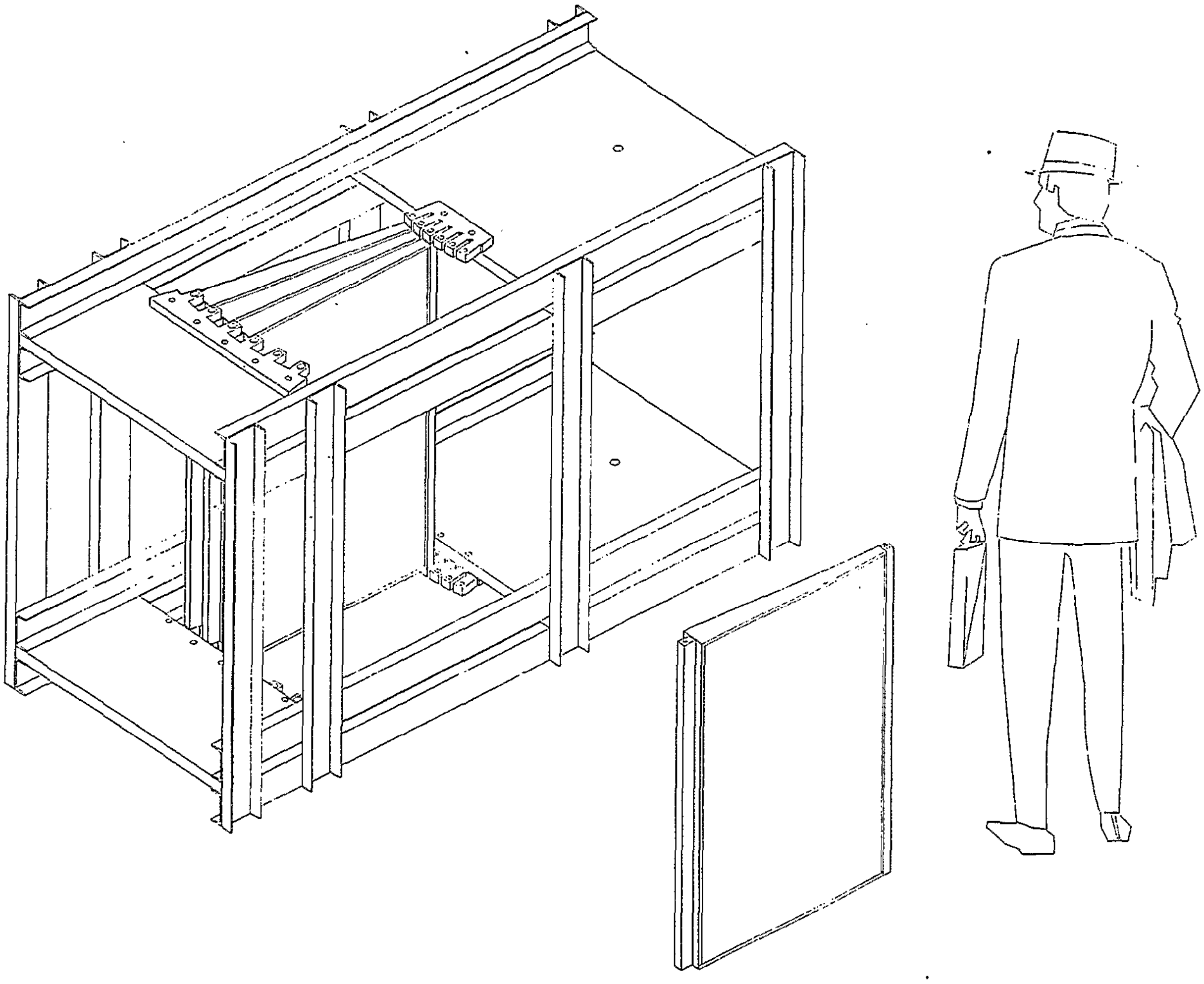

Figure 11: *Sketch of the full scale test frame built for alignment tests.*

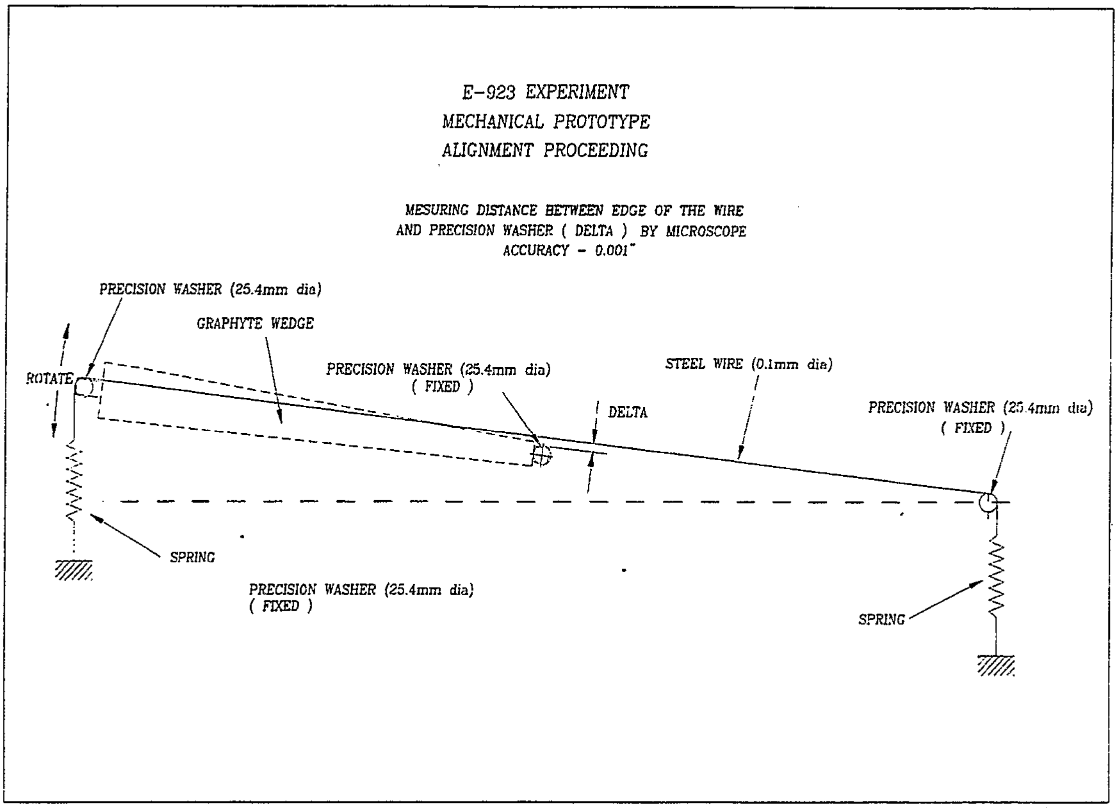

Figure 12: *The alignment procedure.*

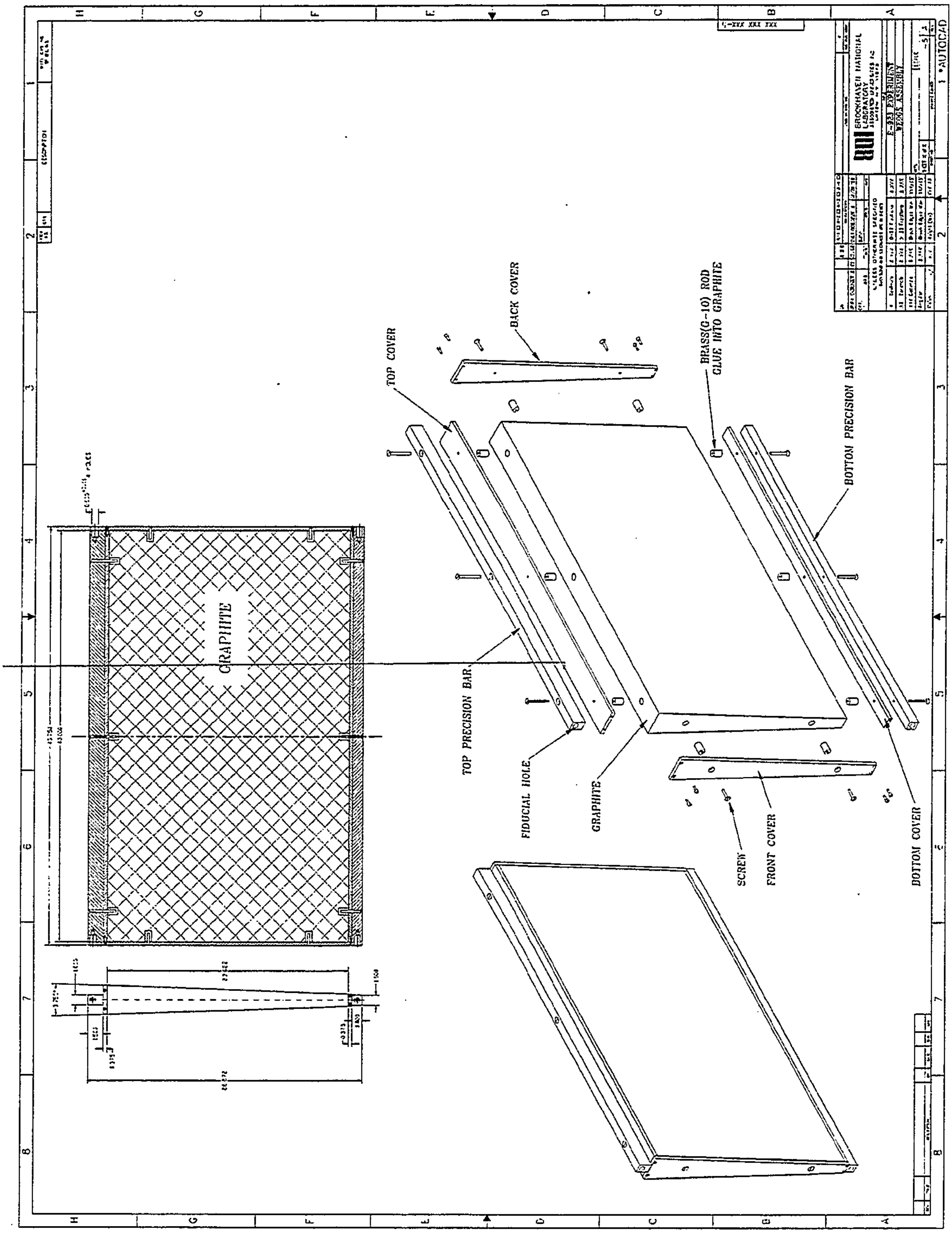

Figure 13: *Preliminary engineering drawing of the polarimeter wedge.*

Sample	Density gm/cc	Asymmetry	Normalized to Ag	Rlxn time μs
Ag		0.2822 ± 0.0004	1	22.7 ± 0.7
1	1.77	0.273 ± 0.001	0.969	12.8 ± 0.6
2	1.78	0.276 ± 0.001	0.977	14.5 ± 0.6
3	1.68	0.276 ± 0.001	0.980	14.9 ± 0.6
4	1.79	0.274 ± 0.001	0.973	13.3 ± 0.6
5	1.72	0.276 ± 0.001	0.976	14.5 ± 0.6

Table 2: *Measured muon decay asymmetry in various samples. 1) Goodfellow (99.95%) graphite rod, 2) Russian sample, 3) Applied Carbon Tech Grade 2020, 4) MWI inc. G330k-P-925, 5) UCAR inc. grade ATJ. The asymmetry reduces over time as* $exp(-(t/\tau)^2)$ *where* τ *is the relaxation time.*

possible analyzing power for the muon polarization. The samples were prepared as discs of diameter 3.175 cm (2.54 cm for sample 1) and thickness of 0.4 cm. They were placed in a 60 gauss magnetic field and exposed to low energy muons that stopped in the samples. Scintillation counters were used to record the spin precession. A sample of silver was used as the standard. The results of the test are tabulated in table 2. We see that any one of these industrial graphite materials can be used in the experiment.

5.3 Polarimeter Chambers

As explained in the E923 proposal the two options for the polarimeter active detector technology are proportional chambers and scintillation counters. We have been developing both options. We intend to choose one when the funding situation for the experiment becomes clear.

Figure 14 shows the schematic of a polarimeter chamber. We have built 4 such chambers. They are currently under-going a variety of tests. The critical issues for the chambers are the total thickness of 9 mm, flatness, and efficiency. These are conflicting requirements: flatness requires thick, strong material in the construction, but efficiency requires keeping the gas gap as large as possible without increasing the total thickness beyond 9 mm.

We have chosen to have two gas gaps on two sides of the central readout plane; 60 cm long 30μm sense wires are wound around this plane with 60 gm of tension. The gas gaps on both sides of the readout plane are 3 mm. Under ideal conditions the instability voltage will be $\sim$ 3000 volts. With P10 gas (90%Ar and 10% methane) the plateau is reached at $\sim$ 1400 volts. The difficulties with the chamber are due to the small gas gap which requires the chamber to be flat within $\sim$ 100μm. If the wire tension on both sides is slightly different due to the winding process, the instability voltage is significantly reduced.

5.4 Polarimeter Scintillator with fiber readout

The second option being considered for the polarimeter active detectors are scintillation counters. As explained in the proposal the advantages of the chambers over the scintillators are (1) the ability to measure the muon range, (2) simpler packaging because the electronics is not sensitive to the magnetic fields whereas photo-multiplier tubes must be placed outside the field. We have devised a scintillator readout system incorporating wave-length shifting fibers that can address both of these problems for a scintillator based active detector. Figure 15 shows a sketch of the scintillating fiber based system. The fibers are embedded in grooves cut into the scintillator plate. A single fiber is looped at one end of the scintillator and both of the free ends are placed on a photo-multiplier tube. The scintillator plane is divided in ten sections along the beam direction to enable measurement of the muon range. The first and last sections of the scintillator can also be used to define the fiducial region for muon decays. The critical issue for this design is the number of photo-electrons and the attenuation in the wave-length shifting fibers.

We have built small prototypes of this concept to test the photo-electron yield. We have built counters with 1mm thick WLS fibers (K27 from Russia) sandwiched between two 4mm thick plates with grooves. The fibers were placed 1 cm apart. With 1.5 m long fibers we obtained a yield of 20 pe/MIP approximately uniform over the 30 cm long and 10 cm wide counter. Although this is adequate for the experiment, we would like to increase the yield to 30 pe/MIP and also design a frame that can hold 10 counters without gaps. The yield can be increased by using better fibers from Bicron or Kuraray. We are also investigating the quality of the grooves and the adhesives used to hold the fibers [13].

5.5 Magnetic Fields

Understanding small magnetic fields is important for the experiment. They need to be understood in the following context: (1) The PMTs must be well-shielded against small fields so that the time delays in the PMT do not depend on the direction of the field to

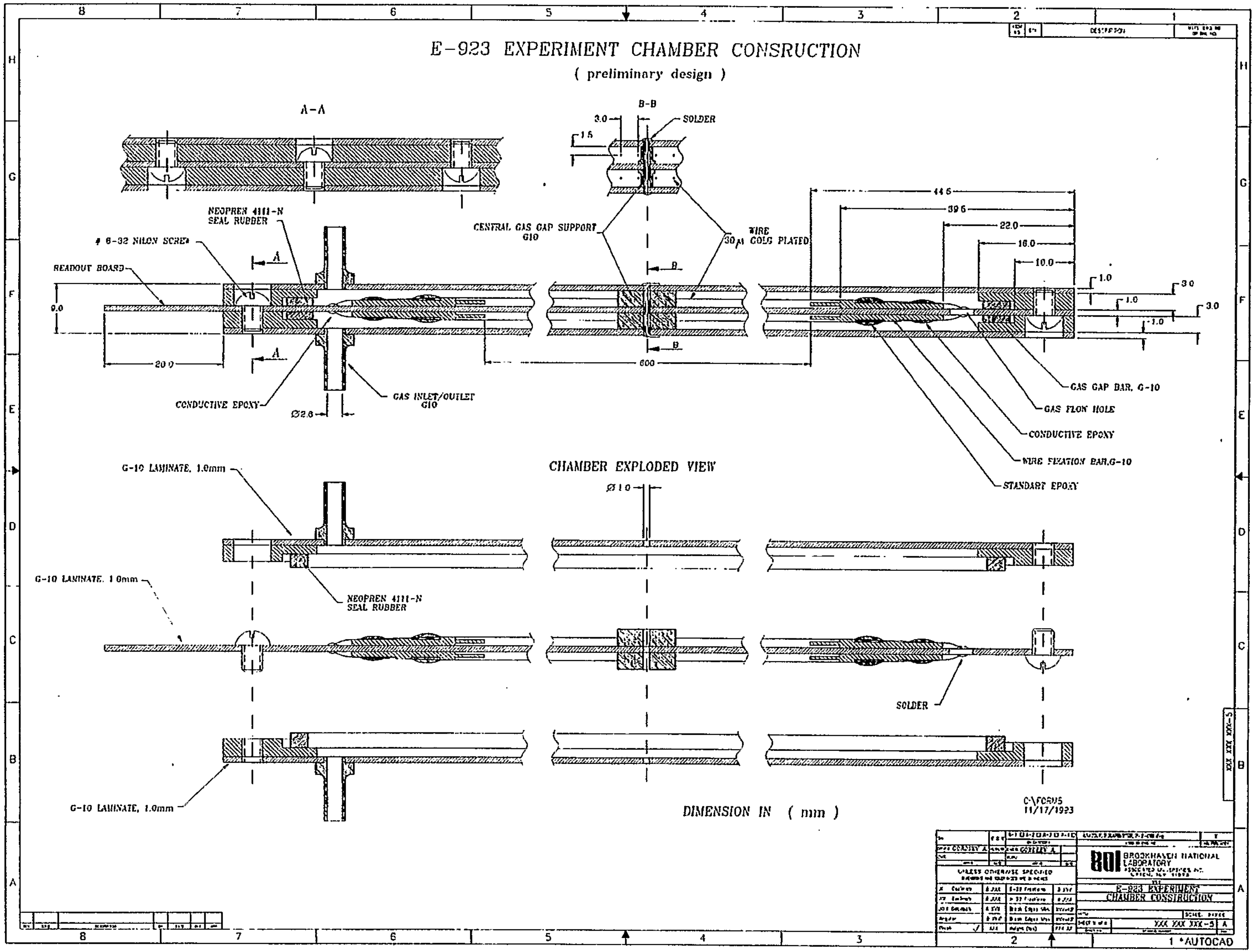

Figure 14: *Engineering drawing of a polarimeter chamber.*

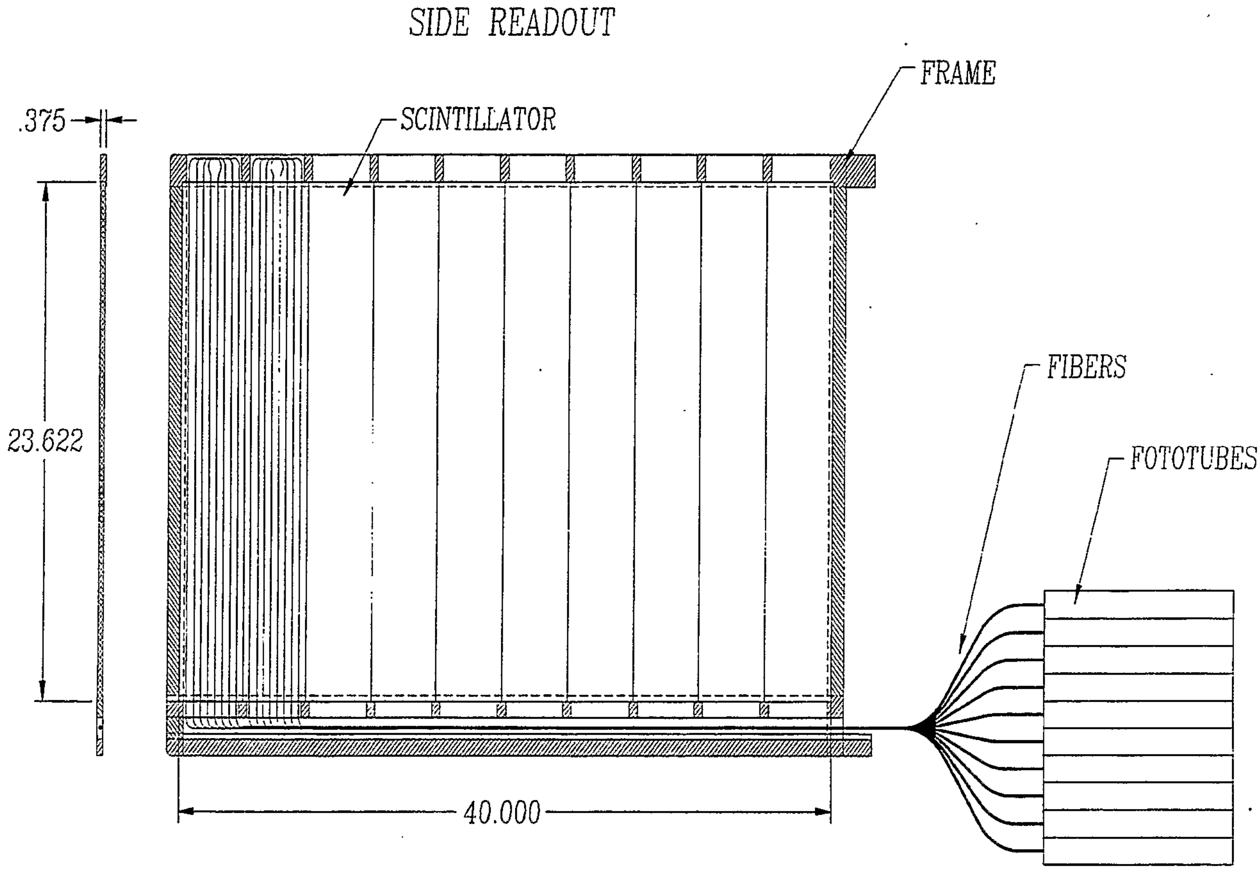

Figure 15: *Sketch of a scintillator based active element in the polarimeter.*

within $\sim 300ps$. (2) The polarimeter must be well shielded against penetration by external fields so that the asymmetry between the magnitudes of the fields is no more than 6 mG. (3) Extra longitudinal fields in the decay region must be kept below $\sim 1Gauss$. (4) The field inside the polarimeter should be uniform to within 5% over the fiducial volume. These issues have been investigated and documented in detail [14].

We have measured the stray magnetic fields in the area of the experiment. The current configuration of the beam line is shown in Fig 16. The fields were measured with a 3-channel (x-y-z) Gauss-meter made by Lakeshore Inc. Model 460 with an accuracy of about 0.05 Gauss. The D6 beamline at that moment was operating at 900 MeV, the AGS was on, the A2 line (E865) and the spectrometer magnet in the A2 line was on. The D6 experimental area had a 48D48 magnet which was also turned on. Table 3 shows the measurements at several points outside the D6 enclosure. We see that the total field is < 1 Gauss throughout the region. The maximum field is at the point nearest the 48D48 magnet. The vertical component is approximately constant at about 0.4 Gauss. The component that is of most concern is the x-component, along the beam, which we estimate to be approximately 0.2 Gauss with the 48D48 magnet removed. The Gauss-meter allowed us to investigate the time dependence of these fields. Slow drifts that changed the fields by $10 - 20\%$ were observed over several seconds, but there was no correlation with the AGS magnet cycle, therefore we conclude that there was no measurable effect from the AGS main ring.

The stray fields along the beam direction in the region seem to be well within our tolerance. The thickness and geometry of the iron shielding on the polarimeter magnet determines the leakage and non-uniformity of the field. With 3/4 inch of shielding iron and a 12 inch hole at the center for the beam we estimate that the field in the fiducial area will not vary by more than 5%. Moreover, the leakage of the external field in the direction of the beam will be less than 0.3 % in the fiducial region. Therefore if the external field is about 1 Gauss, the leakage field will be well within our tolerance. The effect of holes and slots in the end-plates for detector access are being investigated, but should not pose significant problems. We intend to use small diameter PMTs to read out WLS fiber embedded scintillation counters. The fiber based geometry will allow us to shield the PMTs and place them far from the polarimeter magnet. There is concern about small fields from magnetized materials in the polarimeter. We will measure the fields inside the polarimeter accurately to understand the size of these effects.

$3 \cdot 10^{-3} \cdot 0.2$ g

$0.6 \cdot 10^{-3}$ g

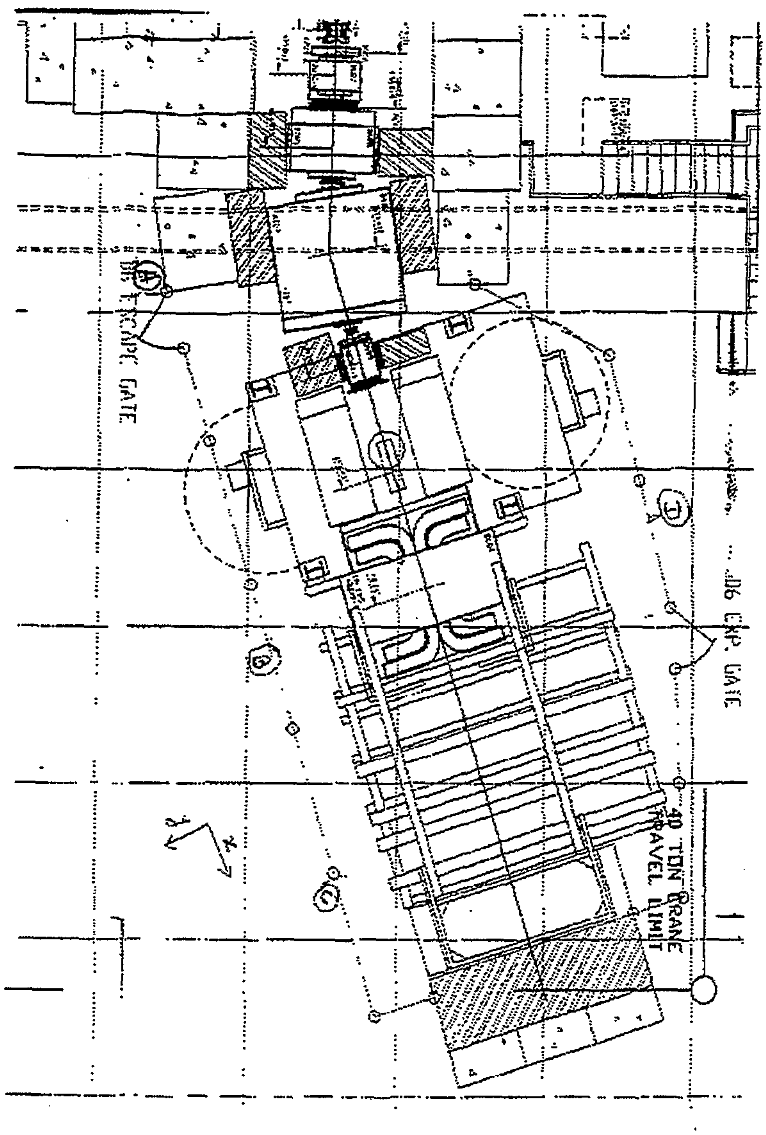

Figure 16: *Drawing of the current configuration in the D6 beam-line, The magnetic field measurements were performed at locations along the fence starting at (A), (B), (C), and (D) and moving away from the fence at various elevations. The beam is at an elevation of 84 inches. The 48D48 magnet was turned on when these measurements were made. The co-ordinate system is indicated in the figure; the z co-ordinate is into the paper.*

Fence Location	Distance from Fence inch	Elevation inch	B_x Gauss	B_y Gauss	B_z Gauss
A	48	84	0.14	-0.08	0.32
		110	0.19	0.08	0.32
	127	84	0.16	0.00	0.37
	200	84	0.22	0.00	0.38
		110	0.16	0.02	0.37
B	26	84	0.87	0.47	0.35
		110	0.73	0.81	0.65
	108	84	0.22	0.21	0.40
		110	0.24	0.23	0.40
C	24	84	-0.05	-0.07	0.38
		110	-0.05	-0.07	0.42
D	27	84	0.26	0.49	0.18
		110	0.36	0.75	0.63

Table 3: *Measurements of Stray magnetic fields in the D6 beamline area. Measurements were performed with a Lakeshore Model 460 3-channel Gaussmeter. The measurement errors are about 0.05 Gauss.*

6 Calorimeter development

Shashlik calorimeter, lead-scintillator sandwich type calorimeter read-out by WLS fibers, has been proposed as the electro-magnetic calorimeter for the E923 experiment. The INR group has developed this calorimeter for the last 10 years, and it should satisfy the main requirements of E923: high rate capability, high stability over a long run (experience of E865), good timing, energy and spatial resolution. The main advantage is much lower cost in comparison with lead-glass or crystal calorimeters.

6.1 Design of E923 prototype module

The design of an individual E923 prototype module developed by our collaboration is shown in Fig. 17. The module is a sandwich of alternating perforated lead and plastic scintillator plates. Cross section size of module is 110mm x 110mm. Each plate of the module has 144 holes arranged in a 12x12 matrix. The diameter of the holes is 1.5 mm in lead and 1.4 to 1.5 mm in scintillator plates. WLS fibers are inserted into these holes. The fiber ends are collected in one bunch, polished, and placed on a 1" diameter photo-multiplier tube. Each fiber is looped at the front of the module, so that both ends of a fiber are on the PMT. Such a loop (radius ~3 cm) works as an ideal mirror with the reflection coefficient ~ 95%. Spacing between fibers is 9.5 mm. White paper (TYVEK) is placed between the lead and scintillator plates. The module is held together with four 50 μm stainless steel strips, one on each side.

6.2 Energy resolution of the shashlik calorimeter

E923 needs accurate measurement of photon energies. Although the main goals of the experiment can be achieved with resolution of $8\%\sqrt{E}$, we would like to have a much higher resolution calorimeter to perform other precision measurements.

6.3 Simulation studies

The estimation of the energy resolution, linearity and uniformity of the shashlik calorimeter modules, as well as optical parameters of light collection was done using GEANT 3.21. The program contains a detailed description of the geometry, following the design of the prototype modules, and includes a description of the light collection efficiency in fibers. Other effects such as attenuation of light in fibers and the photo-electron statistics were included as well. The simulation parameters were tuned by comparing with the results obtained by special test

Type of module	Size of lead plate,mm	Thickness of Sc plate, mm	Number of layers	Total rad. length	rad. length mm	WLS fiber
1	110x110x0.35	110x110x1.5	240	15.5	31.2	1.2mm Russian K-27
2	110x110x0.35	110x110x1.5	240	15.5	31.2	1.0mm BCF-99-29AA (single clad)
3	110x110x0.7	110x110x3.0	120	15.5	30.4	1.2mm Russian K-27
4	110x110x0.7	110x110x3.0	120	15.5	30.4	1.0mm BCF-99-29AA (single clad)

Table 4: *Geometry of 4 shashlik modules considered for beam tests.*

calculations and test measurements. For example, the energy resolution of shashlik module was found to be strongly dependent on GEANT cuts on the lowest electron and photon energies, CUTELE, CUTGAM, respectively. The correction of optical parameters were done after special measurements of light collection efficiency and light collection non-uniformity in scintillator plates. With simulation we were able to separate various contributions to the total resolution: sampling, light collection, etc.

The details of the GEANT simulations will be reported elsewhere. After these simulations four versions of shashlik modules were chosen for experimental tests (see Table 4).

6.4 Experimental studies

Ten shashlik modules with geometry of type 1 and 3 were produced at TECHNOPLAST (Vladimir, Russia) for test measurements. We have used two different types of fibers (K-27 from Russia and BCF-99-29AA from Bicron) and two different types of 1" PMTs (FEU085 and FEU115 from Russia) for the tests. FEU085 is a green-extended PMT with a good quantum efficiency for green light (Q.E. $\sim 15-20\%$). But the maximum anode current of this PMT is limited to $\sim 5\ mA$ per pulse, therefore we have used a fast preamplifier with programmable gain between 2 - 10 for this tube. FEU115 is a standard PMT with Q.E. $\sim 12\%$ for green light and high gain.

The characteristics of the modules were studied by using the B2 test beam at AGS with electrons, pions and muons within the energy range 0.5 - 2 GeV. The prototype calorimeter (matrix 3x3 or nonet) was mounted on a platform which could be moved horizontally and vertically with respect to the beam line. Upstream of the calorimeter, a trigger counter telescope was installed. It consisted of three scintillation counters (S1 - S3). One threshold Cherenkov counter was used to select electrons. The modules were calibrated with 1 GeV electrons. About 1000 electrons were sent into central region of each module at normal incidence. The calibration coefficients were estimated with a precision of 1% from these data. For analysis presented here, all measurement data were corrected with these coefficients.

The energy resolution results described here were obtained by analysis of data taken with the beam position in the central module. The irradiating zone was $12.5mm \times 12.5mm$ as determined by the last counter of the scintillation telescope. The energy spread of the electron beam was estimated to be about 1%. The intensity of the beam was chosen sufficiently low to minimize pile-up and rate effects during the spill. But this requirement was realized only partly, due to the beam size. The beam particle rates for all modules were 50k-100k per spill and pile-up effects had to be taken into account for data analysis. The electronic noise term for nonet of modules was measured during special tests, when calorimeter was removed from the beam. Its contribution to the energy resolution, for all 9 modules is 5 ± 1 MeV. The sum of electronic noise and pile-up effect for nonet of modules was measured in other special beam tests with the trigger gate on the ADC shifted by about 300 ns. The contribution of this noise to the energy resolution, for all 9 modules was 20 ± 3 MeV.

The energy resolution at various energies has been extracted using Gaussian fits and is shown in Fig. 18. We have fitted the measured points to:

$$\sigma/E = (P_1^2 + P_2^2/E + P_3^2/E^2)^{\frac{1}{2}},$$

where P1 represents the constant term, P2 sampling term, and P3 "electronic noise" term to energy resolution. The values of these parameters and GEANT simulation data are shown in the same picture. One sees that experimental and simulation data are in good agreement.

We plan to finish our study of other types of shashlik prototypes by December 1998.

6.5 Electronics of the shashlik calorimeter

The calorimeter readout electronics must store the energy and time of $K^+ \to \mu^+\pi^0\nu$ decay while waiting for the trigger decision after muon decay. This means that readout system must be of the "pipe-line" type with a memory depth of $\sim 6\mu s$. We have completed a preliminary design of this readout system. The electronics architecture is shown in Fig. 19.

We use a LeCroy FASTBUS TDC model 1877s, 96-channel, high resolution (0.5 nsec), Design of Calorimeter module

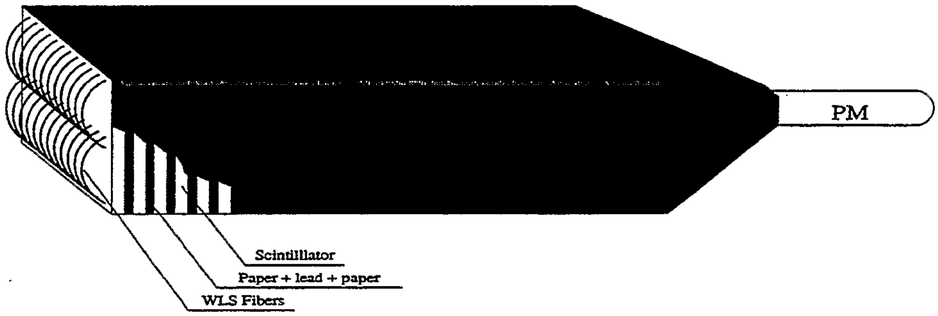

Fig. 1

Figure 17: *Calorimeter module design. The module is a sandwich made of alternating perforated scintillator and lead plates.*

multihit TDC with the depth of LIFO memory from 1 to 16 hits. The 1887s can operate in the common stop mode and provide precise leading and trailing edge time measurement within a time window of 32 μs. The trailing edge can be measured to be as close as 20 nsec to the leading edge. We have designed front end electronics based on the MQT300 chip that can convert an analog signal to a digital signal with the total charge encoded as the width of the digital pulse. With this electronics the 1887s TDC can be used for both time and charge measurement, considerably reducing the cost of electronics for E923. This idea, while extremely attractive, may have unexpected difficulties, therefore we plan to throughly test these ideas in the test beam run in October 1998.

7 Trigger and data acquisition development

The PAC and the technical review had suggested that although the trigger and data acquisition system for the experiment will not be very difficult, we should work on a detailed design. The conceptual design of the system is described in the proposal; we now have a more detailed design of such a system [15].

The trigger is divided in three components. First, a muon stop in the polarimeter is identified. The location of the stop is latched. Then the calorimeter trigger, either 3 clusters

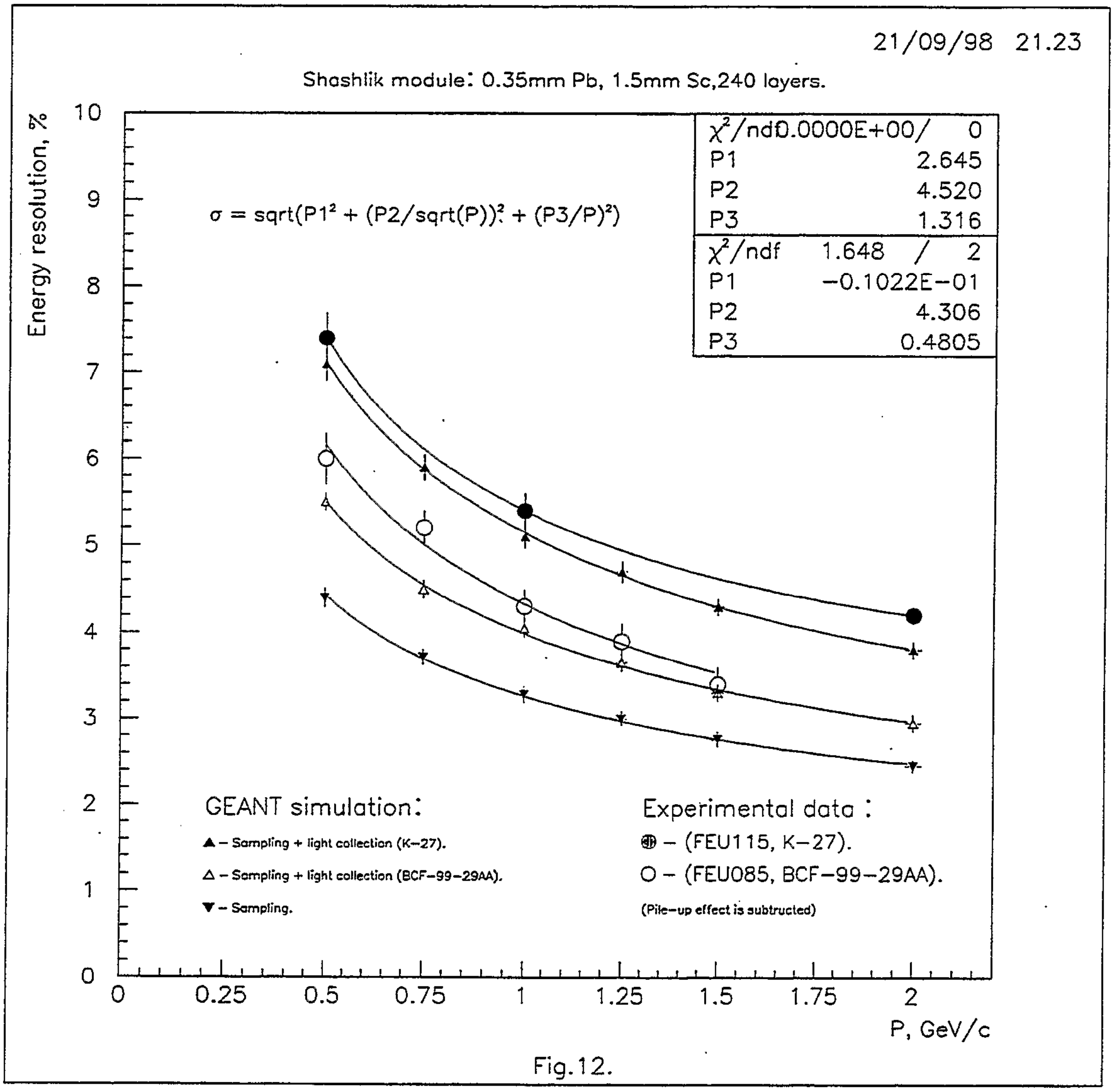

Figure 18: *Calorimeter resolution σ_E/E measured in the BNL test beam. Experimental data (circles) and GEANT simulation (triangles) of shashlik calorimeter energy resolution at various energies. The structure of calorimeter module is 0.35 mm Pb, 1.5 mm Sc, 240 layers. "Pile-up" effect is subtracted from experimental data. The results of the fit for experimental data are given in the upper right hand corner.*

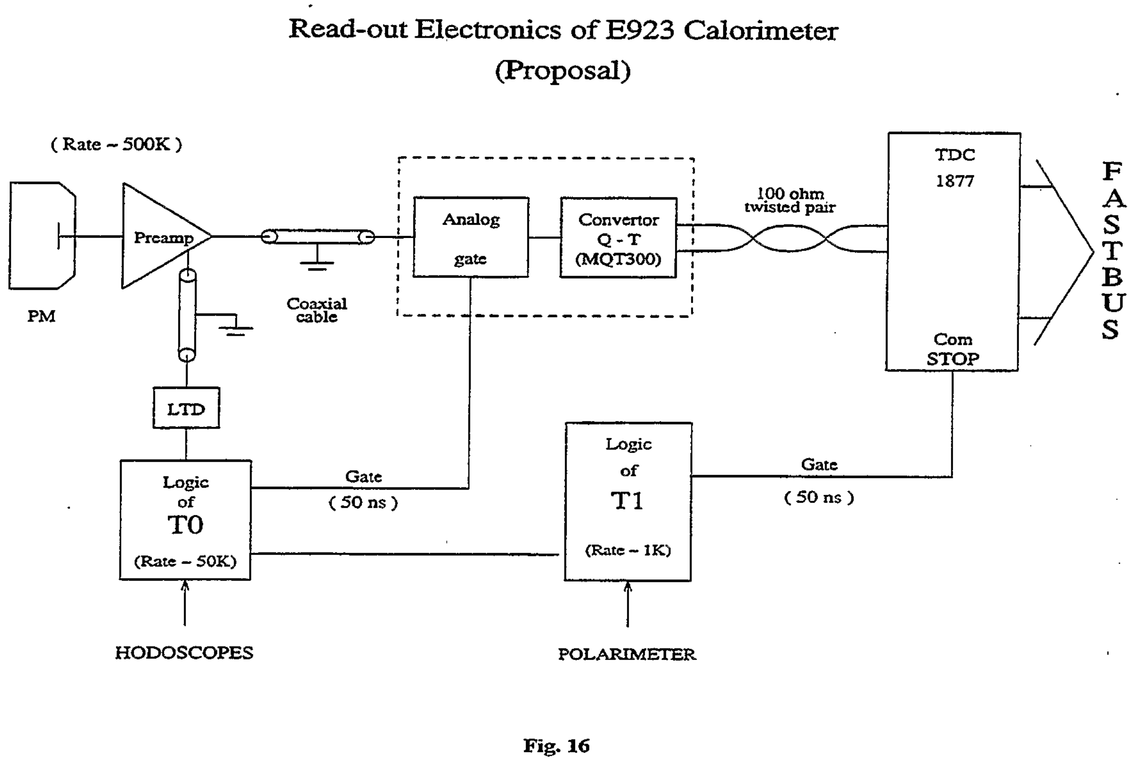

Figure 19: *Proposed calorimeter readout electronics.*

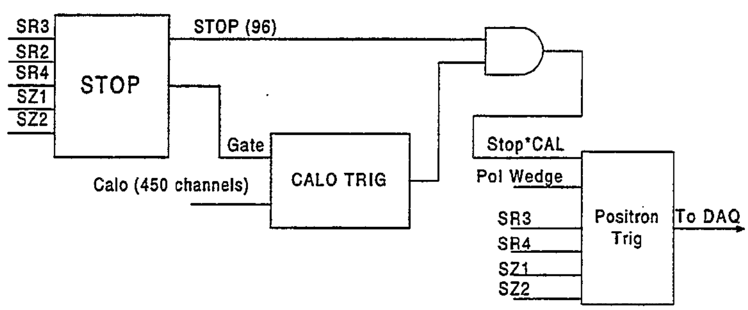

Figure 20: *Overall trigger diagram.*

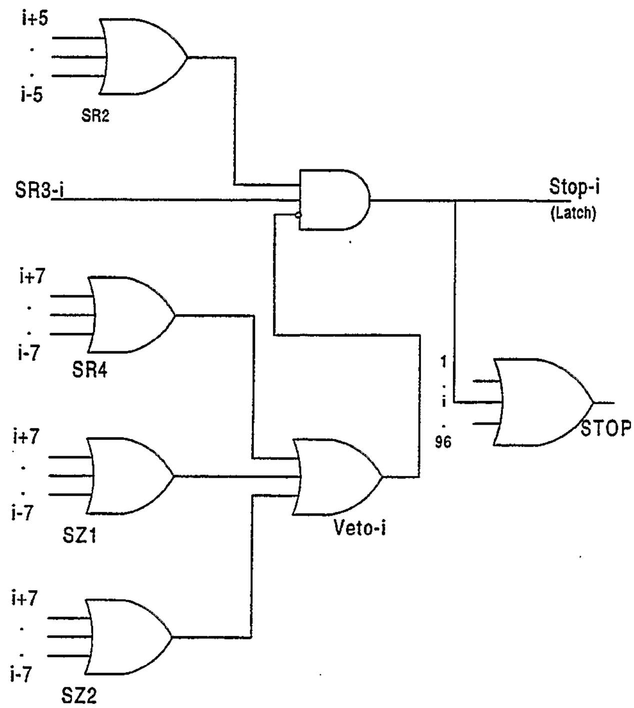

Figure 21: *Trigger logic for muon stop in wedge i.*

or more than 0.5 GeV in the central calorimeter, is required. If both succeed, a positron signal is sought within 6μs near the muon stop. The overall trigger diagram is shown in Fig. 20.

The trigger logic for the muon stop is shown in Fig. 21. Each stop is identified by the associated entrance counter (SR3), which upon acceptance of the trigger by the calorimeter requirement, is latched for further coincidence with the positron signal near the stop. The stop signal contains vetos on counters surrounding the polarimeter. We have simulated multiple scattering of stopping muons to set the number of veto counters for each entrance counter.

The calorimeter electronics is shown in Fig. 22. The calorimeter PMT signal is split in three parts. One goes to the MQT, one to the discriminator for cluster counting trigger, and

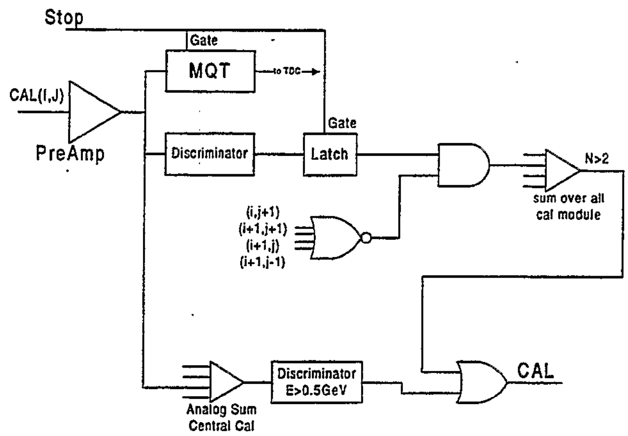

Figure 22: *Calorimeter trigger diagram.*

another for the analog sum. The STOP signal from the polarimeter will provide the gate for integration in MQT, whose output will go to a pipeline TDC (LRS 1877). The MQT converts the analog signal from the calorimeter to a digital signal, the leading edge of which provides the time and the trailing edge provides the amplitude measurement. We have developed and tested this device in the BNL test beam. It will be documented in a future internal note.

The calorimeter discriminator output is latched by a STOP signal. A simple cluster counting algorithm is implemented. The algorithm vetos each module by four of its neighbors on one side. The number of modules that survive is the number of clusters. The threshold will be 30 MeV for each module. In addition to the cluster counting there will also be a trigger based on the analog sum in the central part of the calorimeter.

The positron finding electronics is shown in Fig. 23. The positron signal is defined as a coincidence between hits in neighboring wedges with a difference in Z of no more than 1 segment. Most of these pairs are made by entering or exiting tracks; these tracks must be rejected by vetoing the counters surrounding the polarimeter. The positron signal is required to be within 6 μs and within ±4 wedges of the STOP.

The trigger will be implemented in programmable logic devices, whose common inputs can be shared. The number of channels is reasonably large so that we will have to put the trigger on several identical boards. The design of the implementation is in progress.

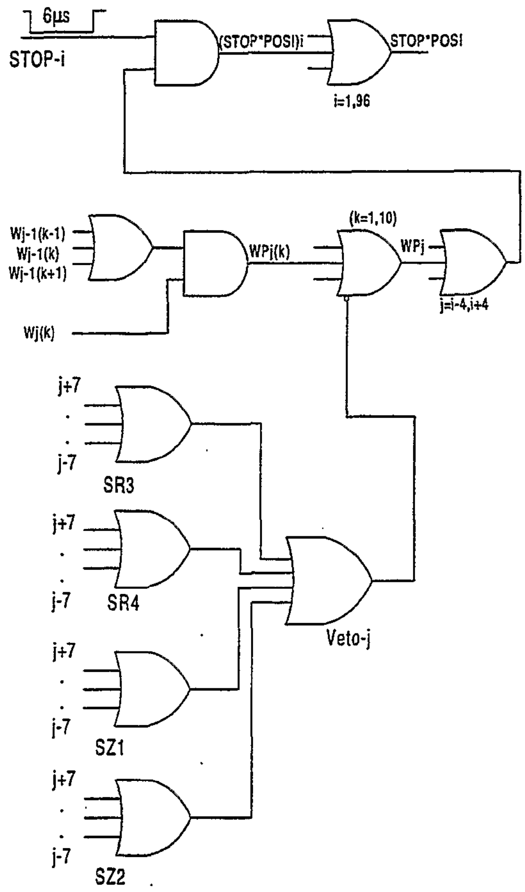

Figure 23: *Trigger logic for positron.* $W_j(k)$ *is the signal from the j'th wedge and k'th segment in Z.* WP_j *is the combined coincidence between j'th and (j-1)'th wedge.*

The readout will be buffered so that the computer readout time does not cause dead-time in the system. The largest dead-time will come from the positron logic which has a 6 μs gate. We estimate this to be about 10%.

The readout design for the experiment will be based on the Struck Fastbus Interface (SFI). The design is shown in Fig. 24. We are working together with the BRAHMS experiment at RHIC on developing this design. BRAHMS has tested a prototype with 1 FASTBUS crate. The readout time from 1 FASTBUS crate has been measured to be

$$T_{readout} = 30\mu s + 200ns \cdot N_{words}$$

where N_{words} is the number of words (4 bytes/word) from that crate. We expect to keep our data rate to approximately 1 kBytes per event. Therefore we do not expect any significant dead-time from the readout.

The design uses ethernet for data transfer to the host computer and commercially available readout and interface electronics. We expect that this choice will make the implementation and debugging much faster and cheaper than a custom system. We expect our data rate to be about 4 Mbytes/spill; the ethernet deign will be able to handle this very easily.

8 Conclusion

The E923 experimental design is based on a previous successful AGS experiment [1]. We have identified the limitations of that experiment and improved upon it. We expect to achieve sensitivity of ~ 0.00013 to the transverse polarization in $K^+ \to \mu^+\pi^0\nu$ decays and ~ 0.0007 to $Im\xi$, an improvement by a factor approximately 40.

The E923 experiment as described in the proposal has gone through a substantial R&D program over the last year. Most of the outstanding issues for achieving the sensitivity for $K^+ \to \mu^+\pi^0\nu$ transverse polarization have been addressed and resolved. The technical review in January 1997 was very helpful to us in motivating and clarifying these issues. They considered our analysis of possible systematic errors thorough and were convinced that a detailed design and implementation of the experiment was feasible.

We have identified other significant physics topics that can be addressed by this experiment. They may require the addition of a photon veto to realize the full potential of the apparatus.

T-violating polarization can be measured in $K^+ \to \mu^+\nu\gamma$ decays with the same experiment. Such a polarization could arise from new effective pseudo-scalar or right handed

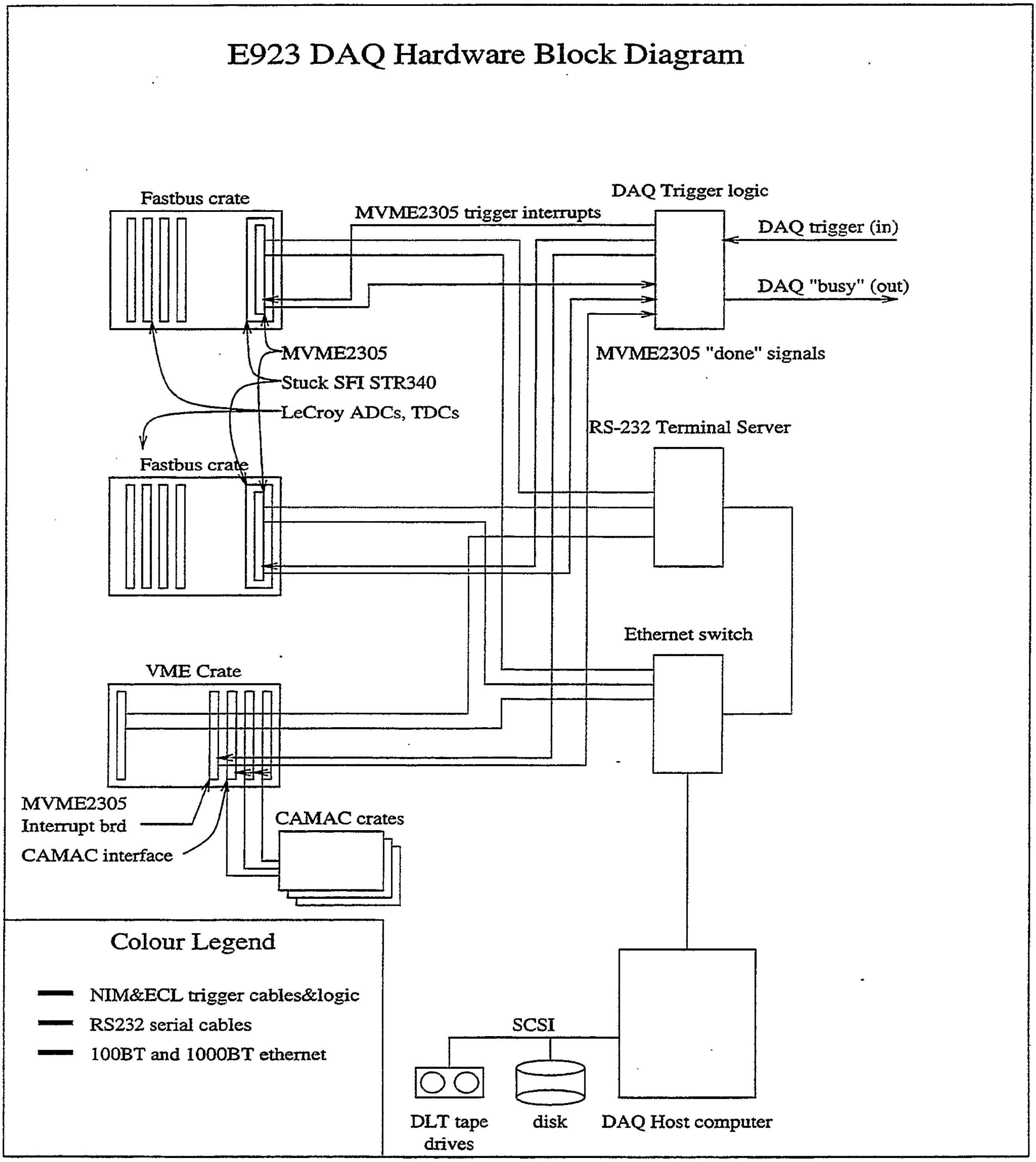

Figure 24: *Overall readout system for E923.*

interactions; therefore the measurement is complimentary to the $K^+ \to \mu^+\pi^0\nu$ measurement. Sensitivity of ≤ 0.001 can be obtained for this polarization. Such a measurement has never been done before; it will also be $\times 10$ better than the current indirect limits on such an effect. The events can be selected from the same triggered event sample as $K^+ \to \mu^+\pi^0\nu$ decays using kinematics and photon veto. The kinematic selection can be made by using the calorimeter and the front tracking chambers. If there is no additional photon veto detector then the sensitivity to the polarization is less, but kinematic cuts can be used to preserve the sensitivity to the underlying physics for pseudo-scalar interactions.

The radiative decay $K^+ \to \pi^+\pi^0\gamma$ can be measured with large statistics in the experiment. Detailed understanding of the Dalitz plot distribution is important as a check on the predictive power of Chiral Perturbation Theory. We can collect 7000 events per hour of this type; there will be 1400 events in the direct emission part of the spectrum and about 150 background. The statistics will be sufficiently large that the systematic issues will most likely dominate the final resolution on the form factors. Without the photon veto we expect the background to be 2 to 3 times higher.

The high intensity separated kaon beam, the polarimeter, and the calorimeter remain the most crucial aspects of this experiment. We have built a 1-1 scale model of a sector of the polarimeter; we have also designed and built the active detectors. These are being tested in the laboratory and the AGS test beam. We have prototyped calorimeter modules that surpass our requirements for most of the physics. We have a design for the data acquisition system and the trigger. Various components of this electronics are currently being tested.

We have sufficient information now to start construction of this experiment. We are in the process of refining the cost and schedule for the experiment. The total preliminary cost estimate is approximately \$3 M in 1998 dollars. The experiment can be completely constructed in 2 years. An initial engineering run could be scheduled after about 16 months. The experiment will need 2000 hours of running time to achieve the main goals. Additional running time may be required for other physics topics.

References

[1] M. Campbell, et al., Phys. Rev. Lett. **47**, 1032 (1981). S. Blatt, et al., Phys. Rev. **D 27**, 1056 (1983). Also see M. Schmidt, et al., Phys. Rev. Lett. **43**, 556 (1979). W. Morse, et al., Phys. Rev. **D 21**, 1750 (1980).

[2] H. Ma, Simulation of the $K_{\mu 3}$ Polarization Experiment —Comparison of two designs, Jan. 11, 1996, Internal Note 6
H. Ma, Simulation of the $K_{\mu 3}$ Polarization Experiment —The baseline design and Radiative $K_{\mu 2}$, Feb. 8 1996, Internal Note 7
H. Ma, E923 Detector Simulation and Radiative $K_{\mu 2}$ decay, September 3, 1998, Internal Note 41

[3] Mark Convery, Princeton University Ph.D. Thesis, 1997

[4] Guo-Hong Wu, John N. Ng, Phys.Rev.D55:2806(1997)

[5] C.H.Chen, C.Q.Geng, C.C.Lih Phys.Rev.D56:6856(1997)

[6] G. Ecker, H. Neufeld, and A. Pich, Nucl. phys, B413 (1994) 321.

[7] R.N. Rogalyov, A.R. Slabospitsky, IHEP Preprint 94-116, Protvino, 1994.

[8] R.J. Abrams et al., Phys. Rev. Lett. 29 (1972) 1118;
V.N. Bolotov et al., Sov. J. Nucl. Phys. 45 (19987) 1023

[9] Hong Ma, Simulation of Experiment 923, Jan 16, 1997, Internal Note 28

[10] Presentations to the technical review panel, Jan 17, 1997, Internal Note 29

[11] C. Pai, A. Gordeev, Some notes on the stress model of the polarimeter, June 15, 1997, Internal Note 36

[12] Robert Adair, Design Considerations for Graphite Machining, March 9, 1998, Internal Note 39

[13] Y. Andreev, Test Beam Results on Scintillator with WLS readout, May 7, 1997, Internal Note 33. Vitaly Semenov, Various documents and plots for WLS fibers, Aug 12, 1998, Internal Note 40.

[14] R. Adair, Calculations of the Magnetic Field in the Polarimeter Precession Magnet, Aug. 10, 1997, Internal Note 35

[15] Hong Ma, Some thoughts on Trigger and Readout in E923, Sep. 14, 1998, Internal Note 42.